NTNU

Norwegian University of
Science and Technology

Source Range Estimation in the Ocean using Time Difference of Multipath Arrivals

Narve Garshol Skurtveit

Master of Science in Electronics
Submission date: June 2016
Supervisor: Hefeng Dong, IET
Co-supervisor: Dag Tollefsen, Forsvarets forskningsinstitutt (FFI)

Norwegian University of Science and Technology
Department of Electronics and Telecommunications

Science, my lad, is made up of mistakes, but
they are mistakes which it is useful to make,
because they lead little by little to the truth.
- Jules Verne

Acknowledgements

I wish to thank Dag Tollefen at FFI for always replying to my questions, review of my work and providing relevant literature. Further, I wish to thank Espen Rustad for linguistic guidance. I want to thank Julie, my fiancè, for always supporting me. I would also like to thank Hefeng Dong for valuable discussion and review of my work. Finally, I would like to thank John Gebbie for answering my questions regarding details of his algorithm.

Abstract

Passive acoustic ranging in the underwater channel is a challenging task. It has been studied and used in military applications such as passive sonar, but also by marine biologists for mammal detection and ranging. Effective passive ranging is challenging due to the complexity of the underwater channel, and the often changing environmental parameters. Most methods also require a long array to estimate bearing and distance at long ranges.

In this project a ranging method based on a ray model is studied. The source range is estimated by comparing differences in signal time arrivals received on two spatially separated hydrophones. The method is applied to data from two bottom moored hydrophones from two different data sets in shallow water: one with the hydrophones moored at 16m depth, the other at 200m. The method provides stable range estimates of surface ships and small boats up to ranges of 700m, in good correspondence with reference data.

Samandrag

Passiv akustisk avastandestimering i havet er utfordrande. Det blir forska på og brukt i militære system som passiv sonar, men også av marin biologar til avstandsestimering av dyr. Passiv avstandsetimering er utfordrande grunna kompleksiteten i havet med stadig endring i dei akustiske parameterane som påverkar utbreiinga av lyd. I dette prosjektet er avstandsestimering basert på ein rettgåande strålemodell studert. Avstanden blir estimert ved å samanlikne målte tidsankomstar frå direkte lyd og overflate/botnreflekter-lyd med modellerte tidsankomstar på to hydrofonar. Avstandsestimata som er presentert er frå to datasett med botnmonterte hydrofonar. I det eine datasettet er hydrofonane på 16 meters djup og på det andre datasettet på 200 meters djup. Metoden gir stabile avstandsestimat ut til 700 m og korresponderar godt med referansedata.

Contents

List of Figures

List of Tables

Chapter 1

Introduction

1.1 Background

1.1.1 Passive ranging

Passive sonar systems use both narrowband and broadband techniques to analyse and investigate the noise radiated by a sound source [15]. By estimating time arrivals a sound source can be ranged. Additionally, through matched field processing a source can be ranged. These methods usually require a relatively large array. Instead of using a large array it is possible to use the characteristics of the underwater channel to gain extra information of a source. In particular the multipath in a shallow channel will provide time delay that can be used to range a sound source.

1.1.2 Ship noise

The signal used for ranging in passive sonar system is the noise radiated from the source. All ships emit sound, mainly from propeller cavitation, but also from flow noise and machinery noise. Large merchant ships have noise at frequencies below 500 Hz. Smaller boats and pleasure craft usually have a larger noise bandwidth, however this is mainly below 6kHz. Examples of ship noise spectra are shown in Figures 1.1 and 1.2 [14].

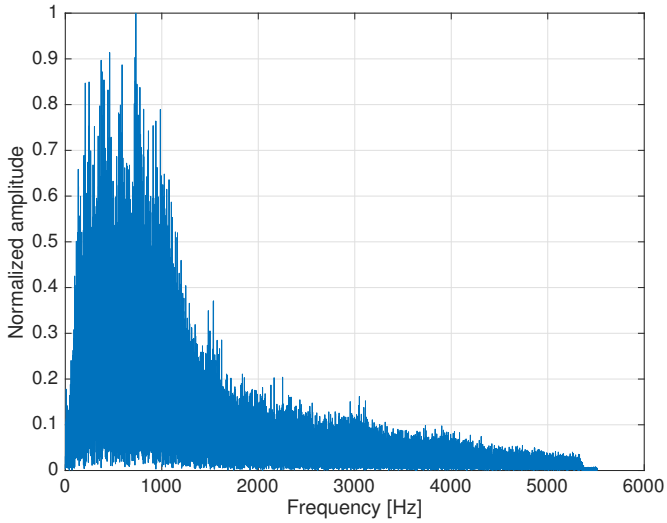

Figure 1.1: Frequency spectrum of noise from an outboard engine

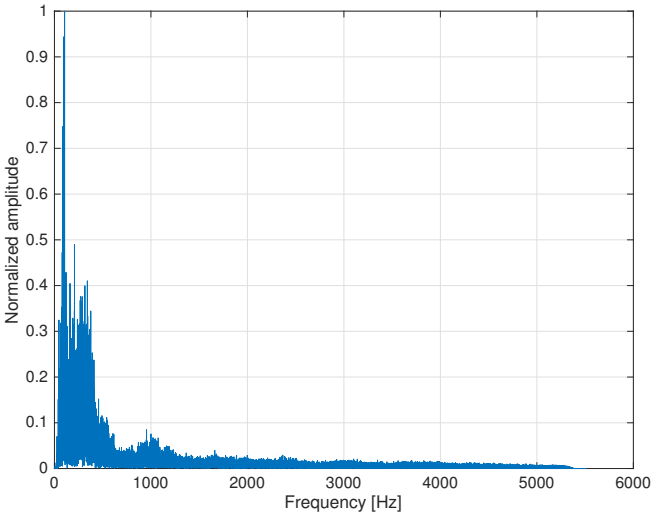

Figure 1.2: Frequency spectrum of noise from a merchant vessel

1.1.3 Acoustic waveguide

The bottom and surface of the ocean create two reflecting surfaces. If the sound speed in the ocean is isotropic in both range and depth, the ocean can be viewed as an acoustic wave guide. With these assumptions the wave equation can be solved analytically, forming the basis of viewing sound as propagating rays [7]. Exploiting the geometry of the channel gives more information than assuming plane waves in free field.

1.2 Thesis

The thesis shall develop a model-based method for the estimation of range to an acoustic source from broadband acoustic data recorded on two hydrophones. In particular, methods estimating time differences of multipath arrivals are of

interest. Relevant measurement data can be from the NILUS sensor platform or an ocean glider and will be provided by FFI.

1.2.1 Motivation

I have worked as an sonar operator on both active and passive sonars. These systems are advanced and the processing methods and algorithms are often hidden from the user. The possibility to process, analyse and program algorithm to interpret raw sonar data provides an unique chance to understanding more of the processing challenges and methods used. On linear array sonars, the range and bearing accuracy is scarce in endfire. In endfire a two hydrophone method will have maximum sensor separation and may produce good range estimates. Range estimation based on a ray model is a simple and fast method. It does not require advanced or expensive equipment. Therefore application of this method on various types of data is of interest.

1.2.2 Outline of method

1. Compute ray trace from sound speed profiles (SSP)
2. Compute correlogram of real data and estimate multipath time delays.
3. Estimate range from given time delay and see if it corresponds with verification data.
4. Estimate relative bearing from receiver to source based on time difference of arrival.

This project is limited to short ranges in an environment being close to isotropic. Ranging will only be studied with the assumption that the source is a surface vessel. The receiver depth is assumed known. The maximum hydrophone separation on the NILUS data is limited to 0.3 m and only two hydrophones are used.

1.2.3 Approach

- Analyse given data and cut out relevant data blocks of ship passing.

- Analyse the spectrum of each source to check bandwidth and possible unwanted noise.
- Produce correlogram [6].
- Filter correlogram to estimate TDOMA.
- Estimate range based on TDOMA by the ambiguity function and the ray model.

All calculation and simulation will be conducted in Matlab v.2015b.

1.2.4 Structure of the thesis

- Chapter 2 describes all theory and formula needed to produce the results.
- Chapter 3 describes the method used to produce the range estimates.
- Chapter 4 describes the Nilus sensor node and the experiment set up.
- The results from the two data sets are presented in chapter 5.
- The results are discussed in chapter 6 and the conclusion is presented in chapter 7.
- Additional results are presented in appendix A, and validation of the ray trace model is presented in appendix B.

Chapter 2

Theory

2.1 Ray model

In a shallow water sound channel the sound radiated by a sound source is reflected by the bottom and surface. Assuming constant sound speed due to the short vertical travel distance from surface to bottom, an image source method can be used to model the acoustic field [1]. By using the simple geometry and automatizing the calculation of the seabed reflection coefficient, the acoustic field can be modelled. Figure 2.1 shows a point source $O_{0,1}$, and a homogeneous layer bounded by the free surface $z = 0$ above, and the bottom $z = h$ below. Superposition of each ray can be obtained at a receiver by calculating travel distance, attenuation and phase shift from each reflection.

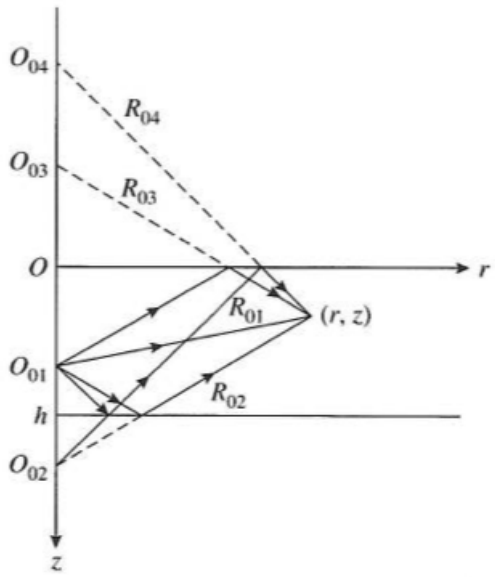

Figure 2.1: Propagation of sound in isotropic acoustic waveguide

Figure 2.1 shows how the ray model can be automatized if rays are grouped in four [1]. where

$$R_{nj} = \sqrt{r^2 + z_{nj}^2}, \quad n = 0, 1, 2...\infty, j = 1, 2, 3, 4 \tag{2.1a}$$

$$z_{n1} = 2hn + z_1 - z, \quad z_{n2} = 2h[n + 1] - z_1 - z \tag{2.1b}$$

$$z_{n3} = 2hn + z_1 + z, \quad z_{n4} = 2h[n + 1] - z_1 + z \tag{2.1c}$$

and

$$\theta_{Inj} = \arcsin(\frac{r}{R_{nj}}) \tag{2.2}$$

$$\theta_{Tnj} = \arcsin(\frac{c_2}{c_1} \cdot \frac{r}{R_{nj}}) \tag{2.3}$$

$$m = \frac{\rho_2}{\rho_1} \tag{2.4a}$$

$$l = \frac{c_1}{c_2} \tag{2.4b}$$

$$V_{nj} = (m \cdot \cos\theta_{Inj} - \frac{l \cdot \cos(\theta_{Tnj})}{m \cdot \cos(\theta_{Inj})} + l \cdot \cos(\theta_{Tnj})) \tag{2.4c}$$

$$\begin{aligned} p_{tot} = \sum_{n=0}^{\infty} \Bigg(& {V_{n,1}}^{(n-1)} \cdot (-1)^{(n-1)}) \cdot \frac{exp(ikR_{n,1})}{R_{n,1}} + {V_{n,2}}^{n} \cdot (-1)^{(n-1)}) \\ & \cdot \frac{exp(ikR_{n,2})}{R_{n,2}} + {V_{n,3}}^{(n-1)} \cdot (-1)^{n} \cdot \frac{exp(ikR_{n,3})}{R_{n,3}} \\ & + {V_{n,4}}^{n} \cdot (-1)^{n} \cdot \frac{exp(ikR_{n,4})}{R_{n,4}} \Bigg) \end{aligned} \tag{2.5}$$

The bottom reflection coefficient V_{nj} can be calculated by equations (2.1), (2.2), (2.3) and (2.4), where r is the horizontal distance, R_{nj} is the ray travel distance, c is the medium sound speed and ρ is the medium density. z_1 is the source depth and z is the receiver depth. $z_{n1} - z_{n4}$ is the vertical travel distance given by the order n and number in group of four j. When each travel distance and reflection coefficient is calculated, the total pressure in a given point can be calculated as the sum of each contribution, as shown in equation (2.5).

2.2 Time Difference Of Multipath Arrival (TDOMA)

In an isotropic channel the arrival structure consists of a single direct eigenray and a series of reflected eigenrays. Working with pulse signals like whale signals make it easy to extract arrival times. However, cavitation from ship noise is continuous and arrival times can not be extracted directly. Cross correlating the signal, the continuous signal is pulse compressed, and differences in arrival times between two hydrophones can be estimated [6]. Time difference of a signal's direct arrival, using two separated hydrophones is defined as TDOA. The time difference between direct arrival and multipath arrivals is defined as TDOMA. These differences are illustrated in Figure 2.3. For first order arrivals they are defined

in Figure 2.2 and 2.3. Note that TDOMA can be between direct arrival at the first hydrophone, and the surface or bottom reflected at the second hydrophone. In theory there are an unlimited number of multipath arrivals, hence TDOMA values. However, the number of higher order arrivals is in practice limited by reflection loss, absorption and the signal to noise ratio.

$$TDOA = \frac{R_{2,d} - R_{1,d}}{c_1} \tag{2.6}$$

$$TDOMA_{bottom} = \frac{R_{2,1st} - R_{1,d}}{c_1} \tag{2.7}$$

$$TDOMA_{surface} = \frac{R_{2,2nd} - R_{1,d}}{c_1} \tag{2.8}$$

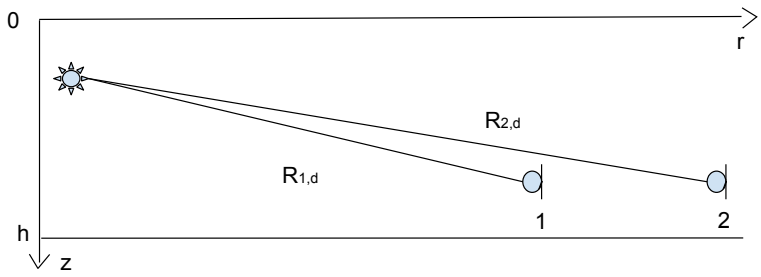

Figure 2.2: Illustration of TDOA represented by travel distance

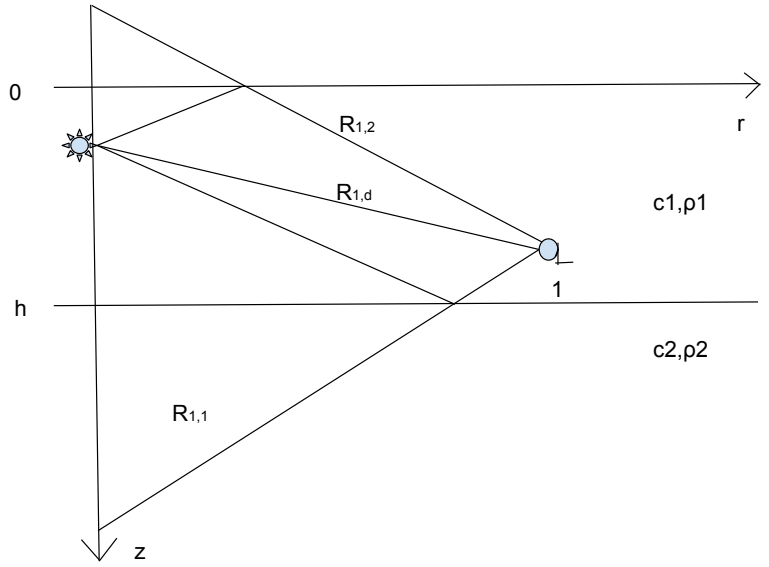

Figure 2.3: Illustration of TDOMA represented by travel distance

2.3 Acoustic processing

2.3.1 Received signal

The signals on two spatially separated hydrophones can be represented by equation (2.9) and equation (2.10). Where the first part is the direct arrival, the second part is the surface reflection and β is the propagation loss relative to the first arrival. The third part is the background noise. y_1 and y_2 represent the received signals on two hydrophones and s is the noise signal from the source. More multipath arrivals could be included, but for simplicity of presentation only the surface reflected ray is included. The noise is modelled as additive uncorrelated Gaussian noise. In this case the sound radiated from a surface vessel is produced by cavitation at the propeller placed near, but beneath the surface.

$$y_1(t) = s(t - t_{1,d}) + \beta s(t - t_{1,m}) + n_1(t) \tag{2.9}$$

$$y_2(t) = s(t - t_{2,d}) + \beta s(t - t_{2,m}) + n_2(t) \tag{2.10}$$

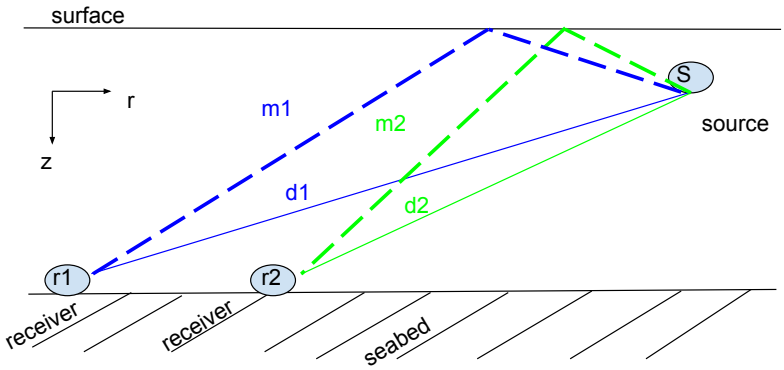

Figure 2.4: Ideally received signal

2.3.2 Finite impulse response (FIR) filtering

A digital signal carries information in the bandwidth of half the sampling frequency according to the Nyquist theorem. Often the complete signal bandwidth is not needed and can be filtered away by using a FIR-filter. A FIR-filter is a filter whose impulse response is of finite length and that settles to zero in finite time, meaning it is stable. It is defined in equation (2.11). In practice it is a convolution between a given signal $x[n]$ and the given filter coefficients b [12]. The filter coefficients are designed to the specific application of the data. This is a simple and stable method of filtering and it is easy to design with linear phase. Parks-McClellan optimal FIR filter design method is implemented in Matlab, and makes it easy to design both efficient and optimal filters using the $firpmord$ command.

$$y[n] = b_0 x[n] + b_1 x[n-1] ..... + b_N [n - N] = \sum_{i=0}^{N} b_i \cdot x[n-i] \tag{2.11}$$

2.3.3 Generalized cross correlation (GCC)

Given the two signals $y_1(t)$ and $y_2(t)$. The discrete cross correlation can be performed in the time domain by equation (2.12), where E denotes expectation. More effectively the same can be performed in the frequency domain by computing the dot product of the Fourier transform of one channel with the conjugate of the Fourier transform of the other channel. Then the inverse Fourier transform of the result is computed. To sharpen the result a weighting function can be implemented. This is to avoid loud tonal components that may stand out in a vessels acoustic signature. The following cross correlation is then defined in equation (2.13) where * denotes complex conjugate and τ the time domain variable. The denominator is the weighting function. The drawback of this method is that only the phase information is preserved. However, in time delay estimation we only need the phase information [8].

$$R_{y1,y2}(\tau) = E[y_1(t)y_2(t-\tau)] \tag{2.12}$$

$$\hat{R}_{y1,y2}(\tau) = \int_{\infty}^{\infty} \frac{Y_1(f)[Y_2(f)]^*}{|Y_1(f)[Y_2(f)]^*|} e^{j2\pi f\tau} df \tag{2.13}$$

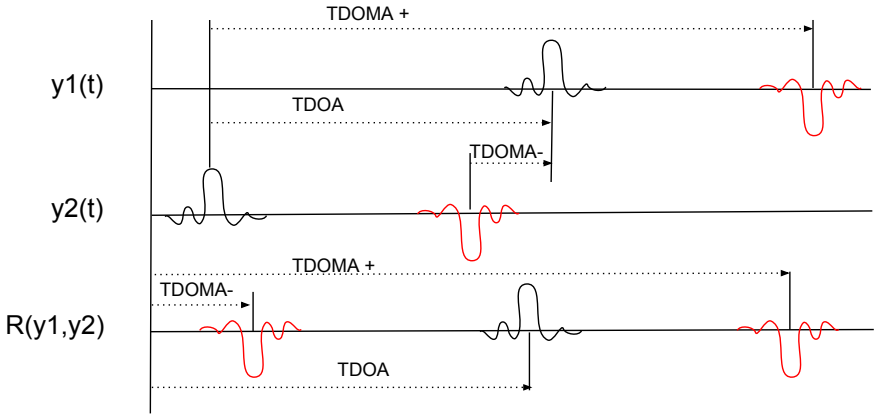

Figure 2.5: Theoretic time arrivals and correlation function

2.3.4 Hilbert transform

A Hilbert transform $\mathcal{H}[y(t)]$ can be viewed as an all pass filter, which shifts the phase of all frequencies $-\pi/2$, making sinus components into cosine components and extending it into the complex plane. The Hilbert transform of a signal $y(t)$ is defined in equation (2.14) where T is the time step variable. This is an improper integral. Therefore the Hilbert transform is properly defined as the *Cauchy principal value* of the integral in equation (2.14)[9]. A real valued signal can be extended into the complex plane where $\mathcal{H}[y(t)]$ is the analytic signal constructed from $y(t)$. The absolute value $|\mathcal{H}[y(t)]|$ gives the envelope of the signal $y(t)$. The Hilbert transform can therefore be effective to compute the envelope of noisy signals. In practice the Hilbert transform can be computed by calculating the Fourier coefficient of a discrete signal, followed by computing the inverse Fourier transform of only the positive valued frequency bins [16]. The Matlab command *hilbert* can also be used directly on a time series to get the corresponding Hilbert transform.

$$\mathcal{H}[y(t)] = y(t) * \frac{1}{\pi t} = \frac{1}{\pi}\int_{-\infty}^{\infty} \frac{g(T)}{t-T} dT = \frac{1}{\pi}\int_{-\infty}^{\infty} \frac{g(t-T)}{T} dT \tag{2.14}$$

2.3.5 Weighted Overlapped Segment Averaging Method (WOSA)

In noisy environments averaging methods may reveal a parameter of interest within a time series. In practise we often have a single time-limited realization of a random process. In our case acoustic data from two different hydrophones. Data from the two hydrophones will be sampled into a sequence of finite length N $y[n] = y[1], y[2], ..., y[N-1]$, with a common clock. The time series of each channel is broken into K non-overlapping segments or snapshots according to equation (2.15) of length M. The snapshots need to satisfy the principle of stationarity, meaning it must be short enough to view the position of the sound source as being fixed. However the snapshot can not be too short, as this will result in less frequency resolution [2].

$$\begin{aligned} y_i[n] = y[n + jM] \quad & j = 0, 1...., K-1 \\ & n = 0, 1, ..., M-1 \end{aligned} \tag{2.15}$$

Sequentially these snapshots are broken into Q overlapping segments of length L according to equation (2.16). Where jD is the starting point for the jth sequence.

Each of these segments are also windowed with a Hanning window to avoid the rectangular window spectral leakage [12]. Note that if D=L the segments are non overlapping, and if $D = L/2$ the segments are 50% overlapping.

$$\begin{aligned} yy_j[m] = y_i[m + kD] \quad & k = 0, 1...., Q - 1 \\ & m = 0, 1, ..., L - 1 \end{aligned} \tag{2.16}$$

The segments are then zero padded to twice the length and the spectrum from each channel is computed resulting in segments of length $2N$. The zero padding is performed to get better spectral resolution, note that this obviously does not increase the time resolution. It is performed to double the number of frequency bins increasing the frequency resolution in the discrete Fourier transform. After this the generalized cross spectrum is computed as described in section 2.3.3. The average over all cross spectrum segments within a snapshot is computed and the inverse Fourier transform of the positive frequencies gives the Hilbert transform of the resulting segment as described in subsection 2.3.4. Averaging a stationary signal in uncorrelated Gaussian noise increases the signal to noise ratio. This produces the envelope of the averaged GCC using the WOSA method. Stacking these cross correlation functions on top of each other produces a correlogram [6]. The correlogram reveals time delays between the two hydrophones.

2.4 Bearing estimation

Based on the TDOA between the hydrophones, the bearing can be estimated if the separation distance is known. The bearing may be calculated according to equation (2.17) where θ is the signal bearing and L the sensor separation distance. The angle θ is measured with respect to the sensor pair axis [4]. The vertical angle α can be calculated in the same way, given that the source is somewhere on the sensor pair axis. The orientation and physical parameters are defined in Figure 2.6. This estimation is correct if the source and receiver is located at the same depth. If not, the vertical angle between receiver and source must be compensated for. Where the vertical angle is defined by equation (2.18) along with the effective separation distance $L_{effective}$. The effective separation equation holds true for both variations in horizontal angle θ as well as vertical angle α. In many cases the horizontal range is much larger than the depth ($r >> z \rightarrow \alpha = 0$) and the vertical angle can be disregarded.

$$\theta = cos^{-1}(\frac{c \cdot TDOA}{L}) \tag{2.17}$$

$$\begin{aligned} \alpha &= tan^{-1}(\frac{d_r - d_s}{r}) \\ L_{effective} &= L \cdot cos(\alpha) \cdot cos(\theta) \end{aligned} \tag{2.18}$$

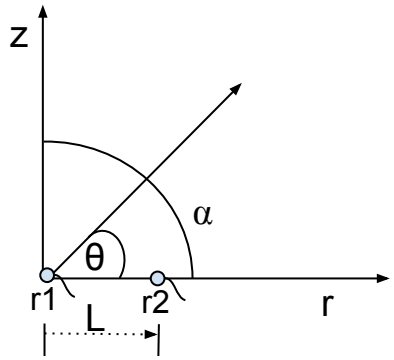

Figure 2.6: Orientation parameters

2.5 Ambiguity function

By comparing or "matching" the estimated TDOA and TDOMAs with modelled TDOA and TDOMAs for a source position x, we can search for the position that provides the best match. To compare data and model, we define a suitable ambiguity function. In this work, we propose the ambiguity function defined in equation (2.19), where τ is the modelled time delay, and $\hat{\tau}$ is the estimated time delay. Index in τ_i runs to the i'th multipath arrival as long as there are readable TDOMA. In most cases τ given by the direct, surface and bottom reflected rays, should be sufficient. σ is defined as $1/2b$, where b is the bandwidth of the signal given in $[Hz]$. The ambiguity function gives results in the range between 0 and 1, where 1 represents perfect match between the measured time delay and the modelled time delay. Maximum value of the ambiguity function ϕ gives the range estimate.

$$\phi(x) = \prod_{\tau=1}^{\tau_i} exp[-(1/2)[[\tau_i - \hat{\tau}_i(x)]/\sigma]^2] \quad i \quad \varepsilon[1, 2, 3...] \tag{2.19}$$

Chapter 3

Method

The following method is developed for NILUS data.

3.1 Data analysis

The data is recorded in large raw files. These raw files were first converted to the wave format. Once in wave format, Adobe Audition was used to navigate the files to search for ship passing. Possible ship passings were located in the time domain representation of the signal as shown in Figure 3.1, and verified by using the Spectral Frequency Display illustrated in Figure 3.2. A ship passing Closest Point of Approach (CPA), will cause a typical bath tub-like plot as shown in Figure 3.2. In Figure 3.2 the x-axis is time, and the y-axis is frequency. The Spectral Frequency Display also gives an indication of the bandwidth of the ship's noise, as well as unwanted noise from other sources. This was later verified by plotting the sound sources' spectrum. These sensor nodes have acoustic communication, and in many cases these communication signals interfered with the broadband ship noise. With this analysis tool, those targets could easily be discarded. The data was then cut into suitable smaller wave-files making it possible to perform signal processing routines without running out of memory on the computer. These wave-files were correlated with available AIS-data and data logs to identify the recordings with the verification data. Once the data was available, a ray trace of both Breidangen and Vealøs (the experiment areas) in Bellhop (the reference raytrace model) and my own ray model was produced, to see what was expected results. After this a algorithm to produce a correlogram was programmed in *Matlab*. This was the most time consuming part as there was a lot of experimenting with filter cut off frequencies, snapshot lengths, segment overlap and segment averaging lengths. During this work I contacted John Gebbie to get tips and reassurance that my data potentially could produce any

results. A synthetic signal from a broadband source in an ideal wave guide was tested to verify the programming. Figure 3.3 shows the GCC from a syntetic signal, and Figure 3.4 show the GCC of a snapshot of Wilson Goole.
A script to easily check a source's bandwidth was coded, to be able to set the best filtering parameters, as well as setting the half width of the Gaussian ambiguity function. Not knowing whether correct programming would produce any readable results, experimenting with cross correlation of each snapshot and averaging in the end was also tested. This gave readable correlogram in some of the data. However, the WOSA method proved best and most effective when filtering and averaging parameters were optimal. Not knowing the orientation of each channel with regard to the source, correlation between all channels was tested to find maximum correlation lag.

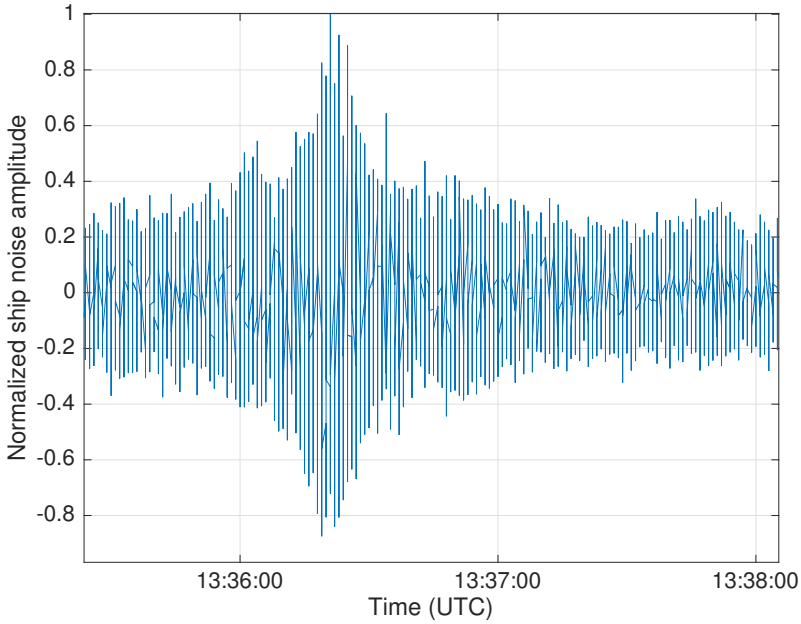

Figure 3.1: Noise signal of Day Cruiser passing CPA

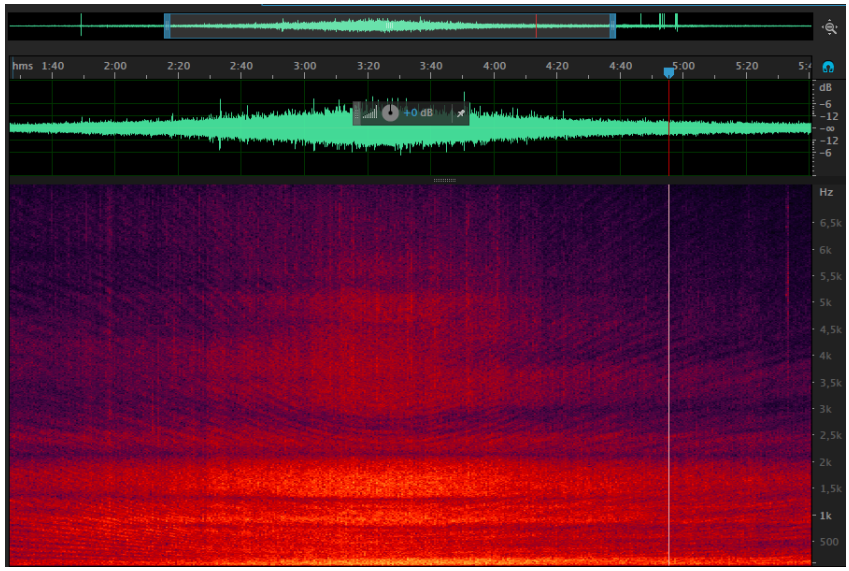

Figure 3.2: Spectral Frequency Display from Adobe Audition of Wilson Goole passing CPA

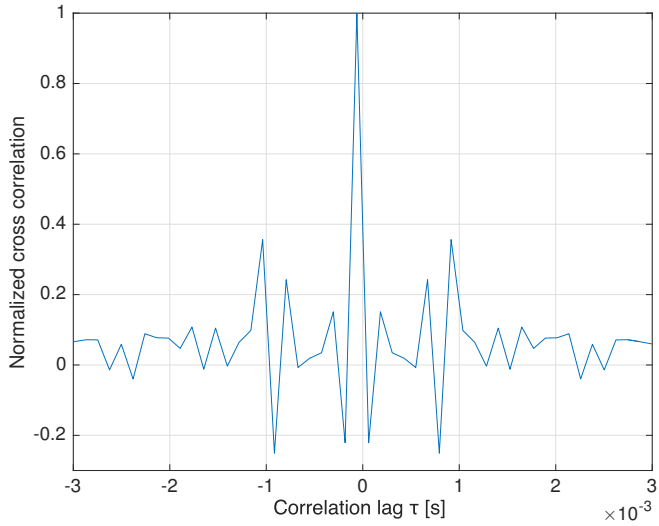

Figure 3.3: GCC from a snapshot of a syntetic broadband signal in an ideal waveguide

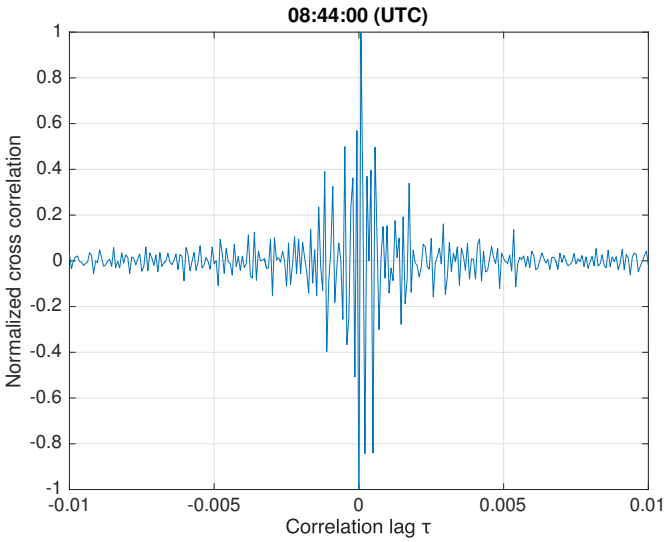

Figure 3.4: GCC from a snapshot of Wilson Goole in Breiangen

3.2 Range estimation

Once readable correlogram was produced, time delays were read from the correlogram. However, it was not obvious which arrivals were visible on the correlogram. Therefore, the different TDOMA possibilities in the given channel were studied to get a first impression sanity check of the results. A TDOMA-table showing the time difference from the surface reflected rays on hydrophone one and the direct rays on hydrophone two are visualized in Figure 3.5. Later, it showed that there were different sets of discernible time arrivals in the two data sets. This is discussed further in Chapter 5. The TDOMA values were extracted from the correlogram using the Matlab command *ginput* which makes it possible to give manual user input from the grid of the correlogram. The ambiguity function was modified to match the right input data with the corresponding TDOA/TDOMA-table. After this the range was estimated by finding the maximum of the ambiguity function's lobe intersecting the surface. A simplified but intuitive flow chart of the method is shown in Figure 3.7. The effective hydrophone separation distance will be updated based on TDOA hence bearing information as shown in

Figure 3.6, if there are readable TDOA.

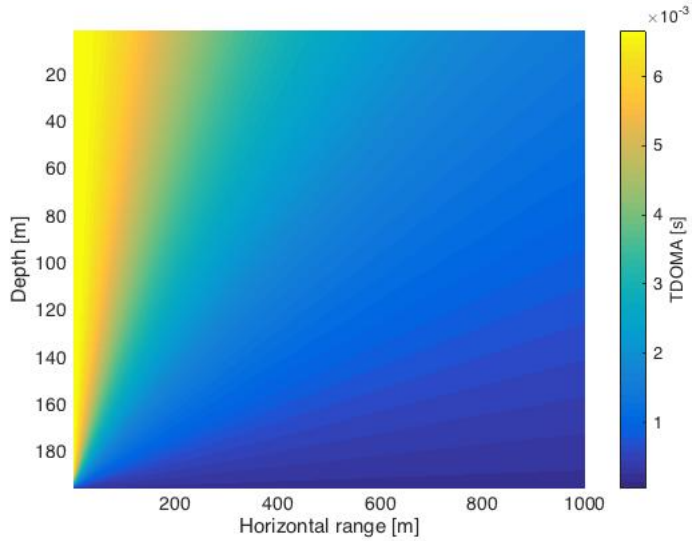

Figure 3.5: Visualized TDOMA table from Breiangen

The true separation distance will also depend on the vertical angle between source and receiver $\alpha = tan^{-1}((d_r - ds)/r)$. However, the horizontal range is usually greater than the difference in source-receiver depth $r >> (d_r - d_s)$ in shallow water, and therefore it is negligible. Still, the TDOA and sound speed at the receiver depth would give the effective hydrophone separation.

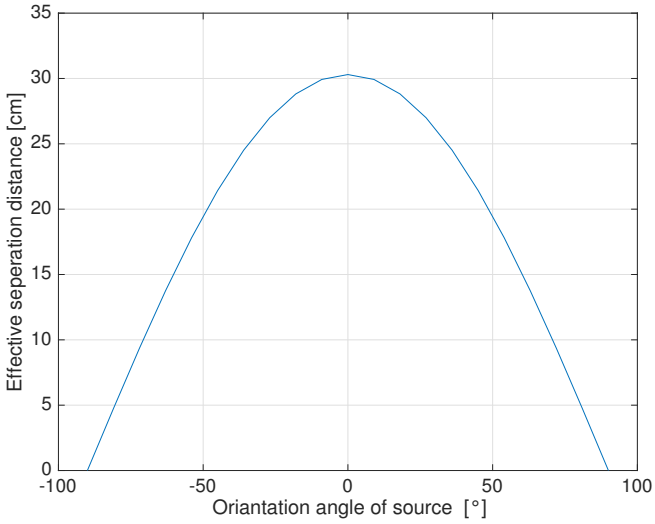

Figure 3.6: Effective hydrophone separation distance

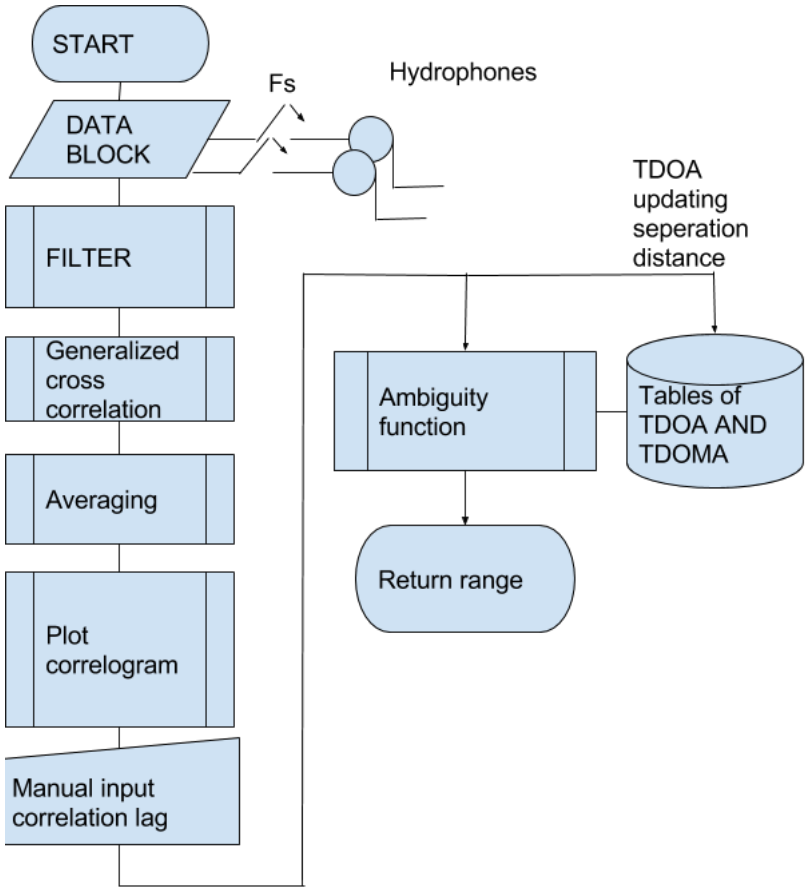

Figure 3.7: Flow chart of range estimation method

Chapter 4

Sensor set up and data set

This chapter describes the Nilus sensor node and the data used. The data comes provided from two different locations, both outside of Horten. The data sets are different both in regards to the sound sources and the channel geometry. Meta data from the relevant ship passings are listed in table A.1 in Appendix A.

4.1 The Nilus sensor node

The Nilus sensor is an easy deployable sensor with communication and local processing capacities. The sensor nodes have passive magnetic and acoustic sensors, and local signal processing which detects passing. The sensor buoys are recoverable by an inflatable liftbag which can be activated remotely [10]. The acoustic data in this work are from a sensor node with 4 hydrophone channels. Arranged in a tetrahedral array, as illustrated in Figure 4.1. The base of the tetrahedron is an equilateral triangle with sides of 30.3 cm which defines the maximum separation distance for the recorded data. Arrays arranged as triplets makes it possible to measure time delay between 3 hydrophones which may resolve left/right bearing ambiguity. However, the method needs a fairly large array diameter to produce measurable time delays[15]. For range estimation the two hydrophones that have the largest separation relative to the source will be used.

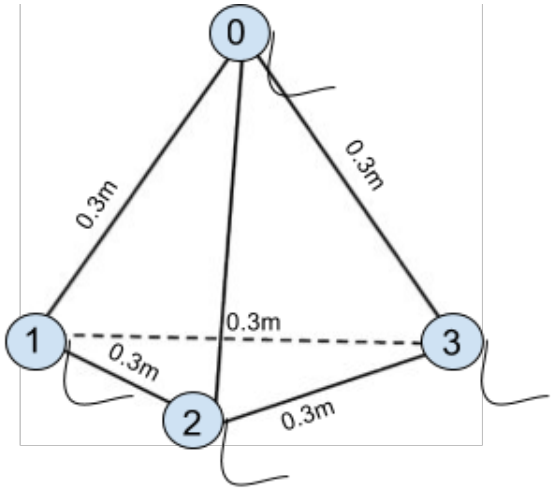

Figure 4.1: Tetrahydron sensor node

4.2 NGAS - 10 June 2010

The sensor buoy was located at an approximate depth of 200m in the merchant ship lane. Figure 4.2 shows the location of the buoy and the bottom profile surrounding it. The bottom around the buoy is relatively flat. The merchant vessels passing Breiangen provides strong low frequent acoustic noise. The Breiangen recordings are recorded with a sampling frequency of $Fs = 14400Hz$. This sample rate gives a minimum measurable TDOA of 2.88 samples (equivalent to 0.2ms) according to equation (4.1). This makes it challenging to detect TDOA. In equation (4.1) $L_{effective}$ was set to 0.3m and c the sea water sound speed was set to 1500 m/s. Range information from this data set is from AIS. Only a few passings from this data set was satisfying because of acoustic communication noise, and other vessels interfering with the recordings.

$$\frac{L_{effective}}{c} \cdot Fs = TDOA \tag{4.1}$$

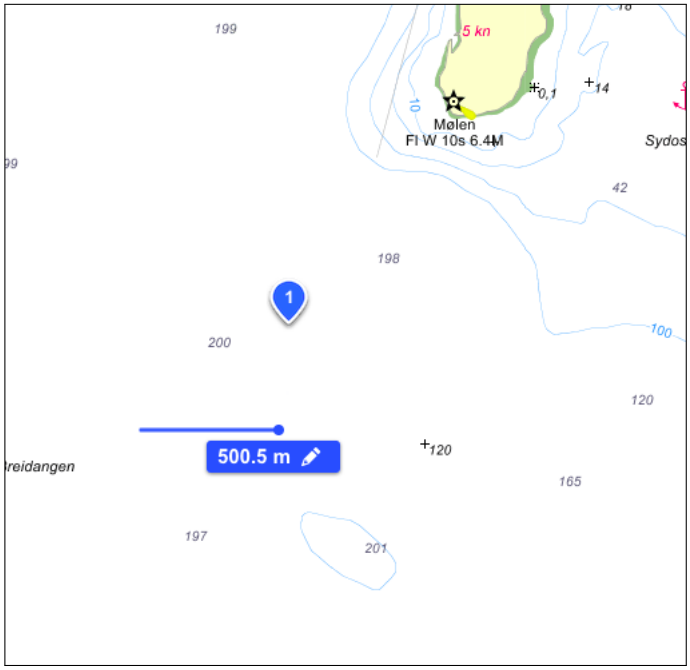

Figure 4.2: Bathymetry Breiangen

4.3 Vealøs - 24 June 2014

Vealøs is outside of the narrow and shallow channel into Horten inner harbour shown in Figure 4.3. The sensor buoy was placed at 16m depth marked in Figure 4.3. In this area mainly small boats pass, and the bottom in the vicinity of the buoy is relatively flat. Vealøs provides more broadband sources. The recordings from Vealøs are recorded at $Fs = 18000Hz$. At this sampling frequency the maximum possible TDOA is 3.6 samples according to equation (4.1).

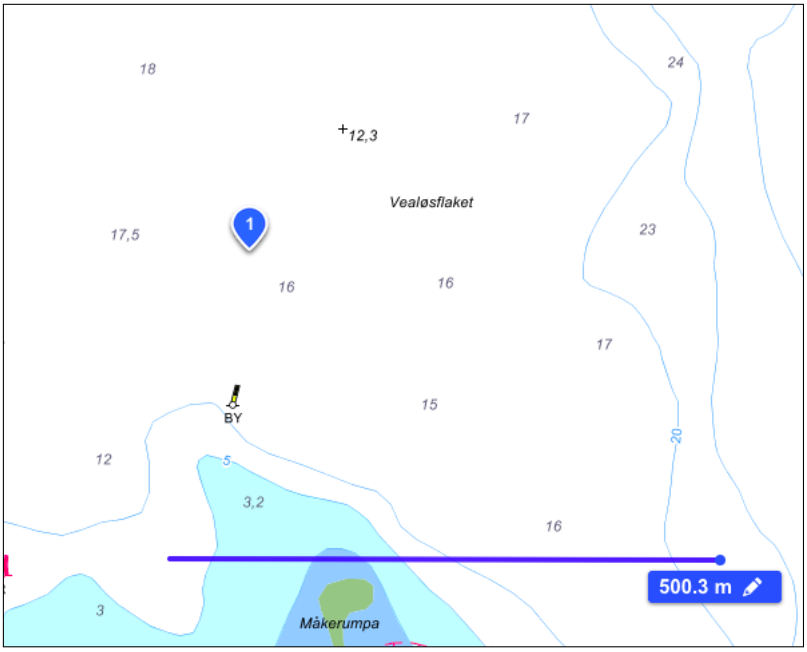

Figure 4.3: Bathymetry Vealøsflaket

4.4 Theoretic TDOMA

4.4.1 TDOMA with surface reflected rays

Figure 4.4 shows expected TDOMA for a ship passing closest point of approach (CPA) in Breiangen. The plot is based on the geometry given in Breiangen and the TDOMA between the direct ray and the surface reflected ray, as shown in Figure 2.4. The plot was computed with a source depth of 5m, which is typical assumed source depths of merchant vessels.

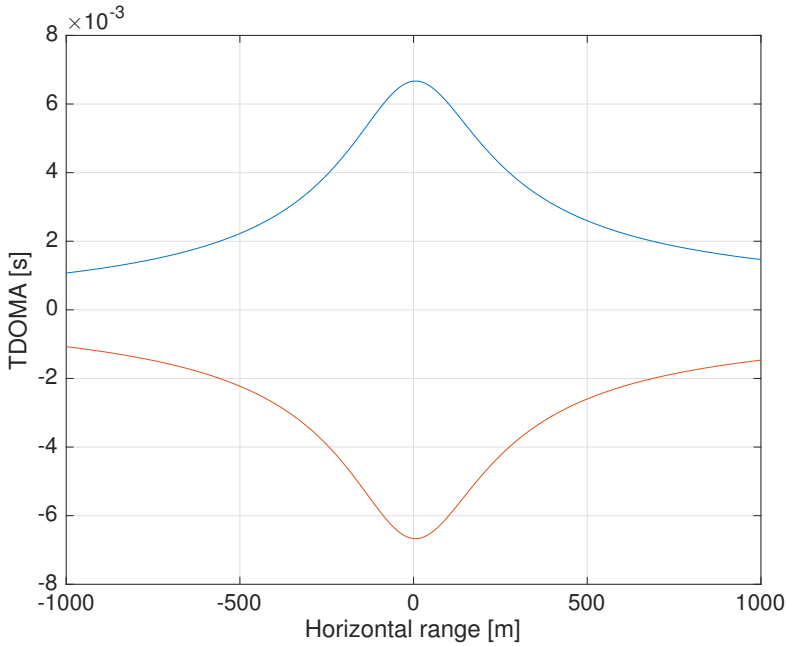

Figure 4.4: Theoretic TDOMA of ship passing CPA, for two possible multipath arrivals, for the Breiangen experiment

4.4.2 TDOMA from surface reflected rays with depth dependence

Figure 4.5 shows the TDOMA for the surface reflected and direct rays. Three different source depths are plotted to illustrate the effect of change of the source depth. A small change in source depth changes the values of the TDOMA from the surface reflected.

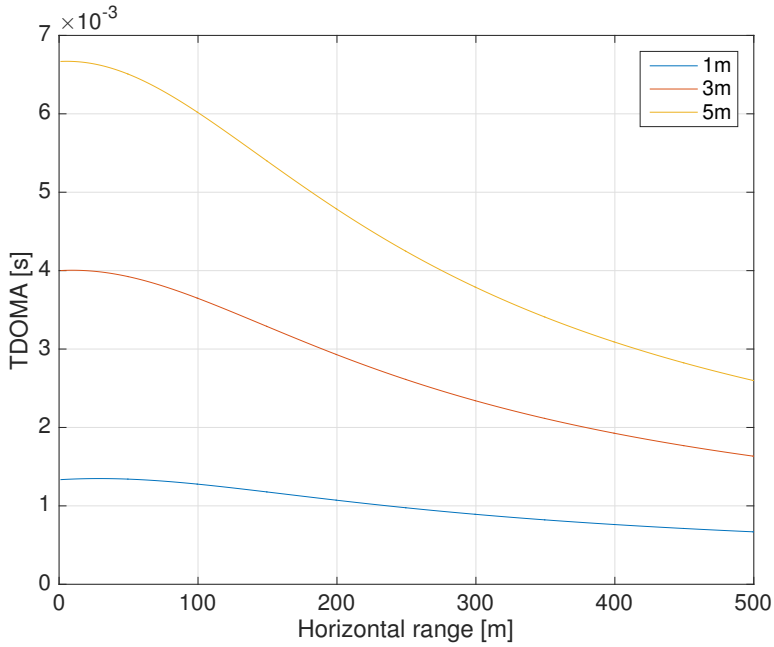

Figure 4.5: TDOMA of surface reflected rays in Breiangen, with varying source depth

4.4.3 TDOMA from bottom and surface reflected rays with depth dependence

If the signal to noise is sufficient, the bottom and surface reflected ray will be readable. This parameter is plotted in Figure 4.6 with varying source depth. The time difference plotted is between the direct and the bottom and surface reflected rays. This parameter is less sensitive to the uncertainty of the source depth.

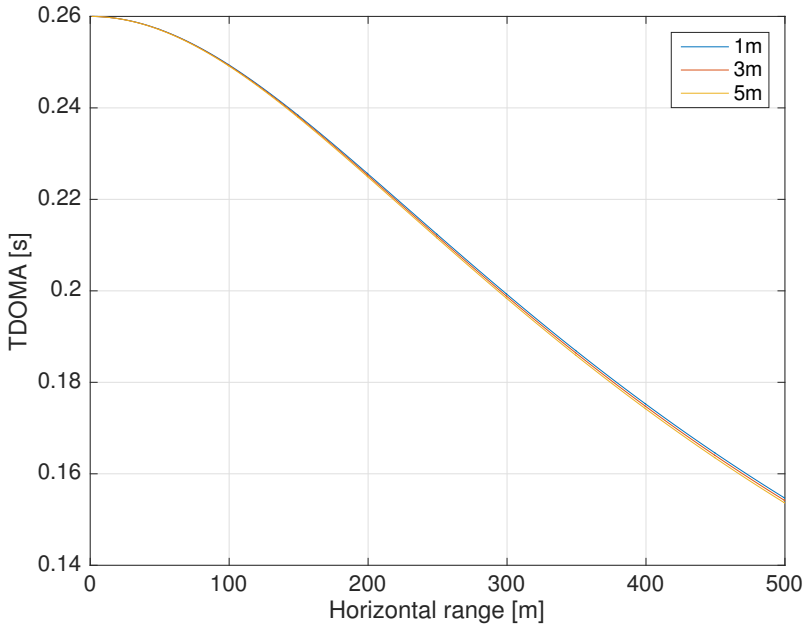

Figure 4.6: TDOMA of bottom and surface reflected rays in Breiangen, with varying source depth

4.5 Stationary signal

The ship's radiated noise is not a stationary signal. However, by time limiting the snapshots being processed from the data the signal can be viewed as temporally stationary. As an assumption most vessels travel up to speeds of 10m/s. In half a second the maximum change in horizontal range possible relative to the sensor node will then be 5m. The vessel would then have a course pointing to the sensor node. Snapshots of half a second allows snapshot lengths of $Fs/2$ samples, where Fs is the sampling frequency. As a rule of thumb the signal is assumed stationary within half a second.

Chapter 5

Results

In this section the results from the two data sets are presented. A total of 12 vessels passing the sensor node from the two data sets was studied. However only the correlogram that provided readable results (in terms of measurable TDOMAs) is presented. The relevant normalized spectrum, correlogram and range estimate is presented.

5.1 NGAS 10 June 2010

The channel parameters for the Breiangen data are listed in table 5.1. The SSP for the area is shown in Figure 5.1 along with a ray trace produced with the Bellhop raytrace model [11]. The SSP shows a layer around 10m and a weak sound channel at 30m. Deeper the SSP has a weak positive gradient. This is a typical summer SSP, where sun heats the top layers, and deeper the sound speed decreases because of temperature to a certain point, where the pressure makes the sound speed rise. The ray trace also shows that in a horizontal range of $1000m$, the rays are little affected by refraction. Some of the rays that are launched in the horizontal direction are caught above the layer. The rays penetrating the layer are travelling close to direct. Note that the ray trace is computed with only 30 rays, whereas a real source will send rays continuous in all directions. Figure 5.2 shows relevant eigenrays contributing on a receiver placed at 400m horizontal range from a source.

Table 5.1: Channel parameters Breiangen

Depth	200 m
Receiver depth	200 m
Source depth	5 m

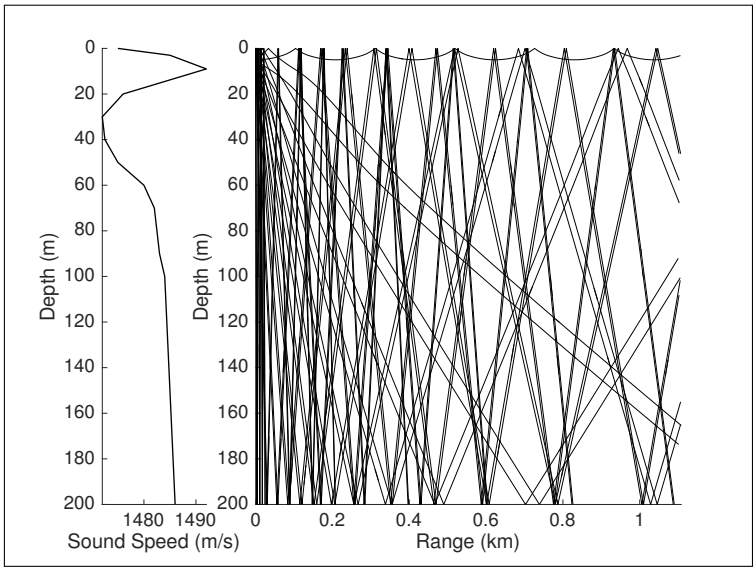

Figure 5.1: Bellhop ray trace from Breiangen

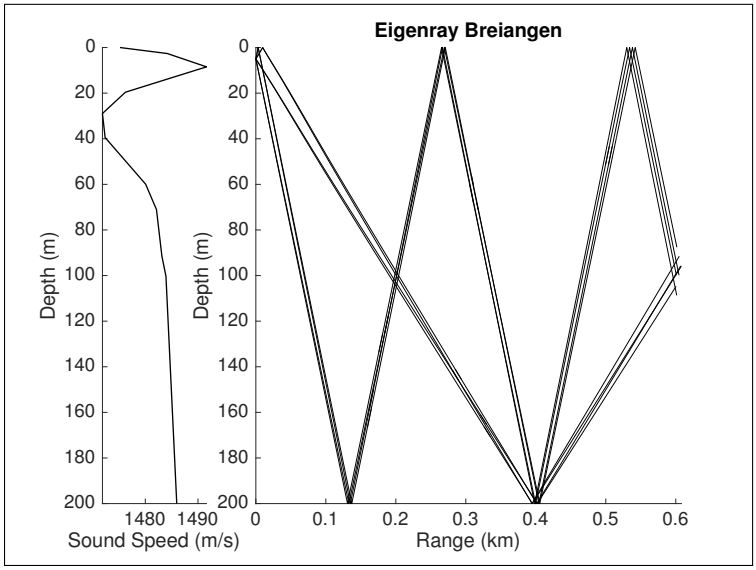

Figure 5.2: Bellhop eigenray computation from Breiangen

5.1.1 Wilson Goole

Figure 5.3: Wilson Goole

Table 5.2: AIS data Wilson Goole

CPA	147 m
Class	Merchant vessel
Draft	5.8 m
Speed	11,6 m/s

The spectrum is shown to see the sources' noise bandwidth. The signal bandwidth is inversely proportional with the half width of the Gaussian in the ambiguity function defined in equation (2.19). Therefore the spectrum is important to decide

the noise bandwidth. The ambiguity result for Wilson Goole at CPA is presented to illustrate range estimation using the ambiguity function. The signal spectrum of the cargo ship Wilson Goole is shown in Figure 5.4. The vessel's radiated noise is mainly below 2kHz, however with some stronger frequency components around 4kHz. The bandwidth of the signal was therefore chosen to 5kHz, and a appropriated filter was designed.

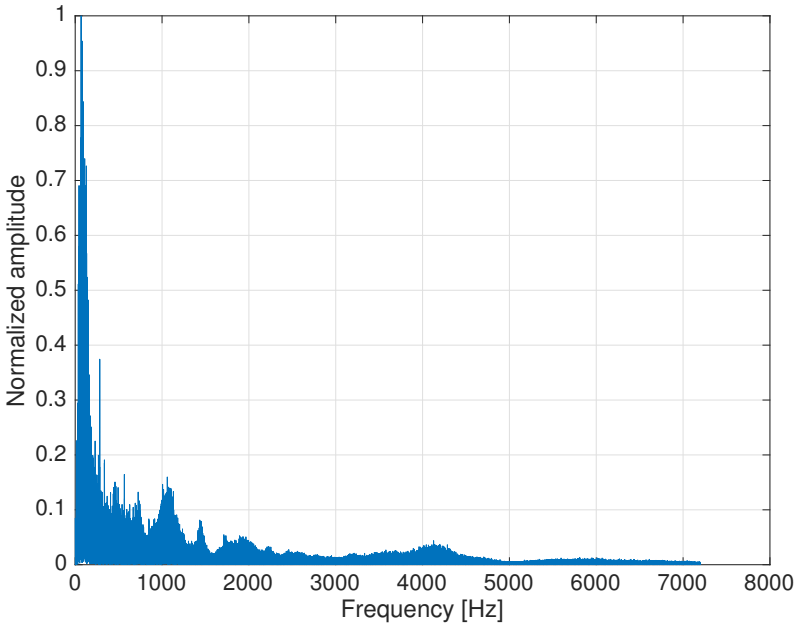

Figure 5.4: Frequency spectrum of noise from Wilson Goole

Figure 5.5 shows the correlogram from processing of data from Wilson Goole passing CPA. The contours of the time delay increase towards CPA and decrease after passing CPA in accordance with modelled TDOMAs shown in Figure 4.4. This is as anticipated when TDOMA was studied and modeled in the project thesis [13]. The TDOMA decreases rapidly outside of CPA and is fast smeared into the TDOA main correlation at $\tau = 0$. Due to small sensor separation and low sampling frequency, the TDOA measurement was not sufficient to update effective sensor separation. Therefore the effective sensor separation was set to 0.3m. The correlogram shows two delay curves at each side of $\tau = 0$, however

only the closest curve to $\tau = 0$ correlates with the channel geometry. The outer curve is assumed to be processing ringing. Different methods were tried to get rid of processing ringing, including windowing of snapshots prior to GCC-processing and also windowing was performed on the averaged cross spectrum in the pass band prior to the inverse Fourier transform [5]. However, it proved difficult to get rid of all ringing. Searching automatically for maximum proved difficult in each snapshot, therefore visual extraction with the *ginput* command was used to get the TDOMA readings that are visualized in Figure 5.6. This data was given as input to the ranging algorithm, which matched predicted TDOMA with the input data.

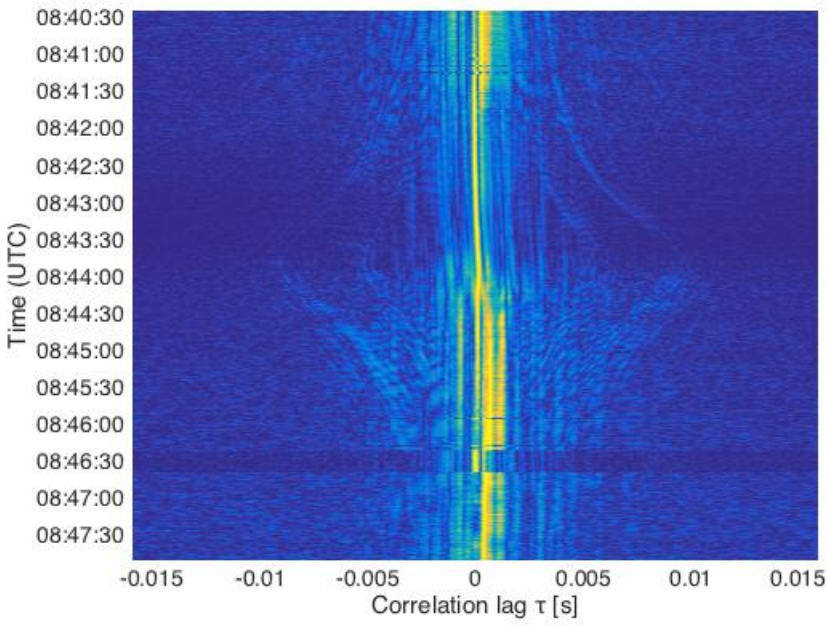

Figure 5.5: Correlogram from Wilson Goole

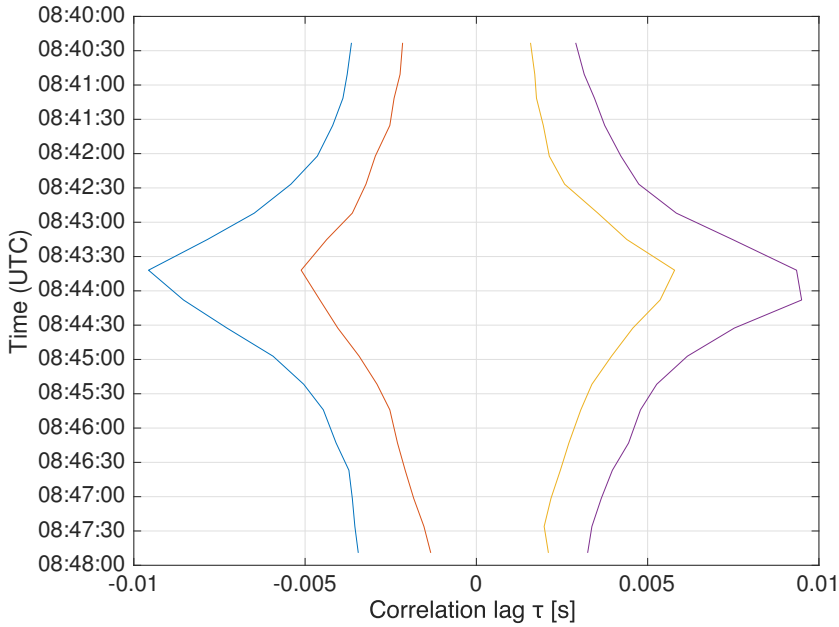

Figure 5.6: Extraction of TDOMA from correlogram

The ambiguity plot is shown in Figures 5.7-5.9. This is based on the TDOMA reading at CPA, equivalent with the maximum TDOMA value. Figure 5.8 shows the source depth uncertainty of a surface vessel, in this example set to 3m. To get unambiguous range estimates the source is assumed to be a surface ship. AIS gives the draught, however the actual source depth is unknown. This is included in the ambiguity function as a surface layer of the value 1. The intersection between the source depth uncertainty and the ambiguity function based on the surface reflected ray produces the total ambiguity function shown in Figure 5.9.

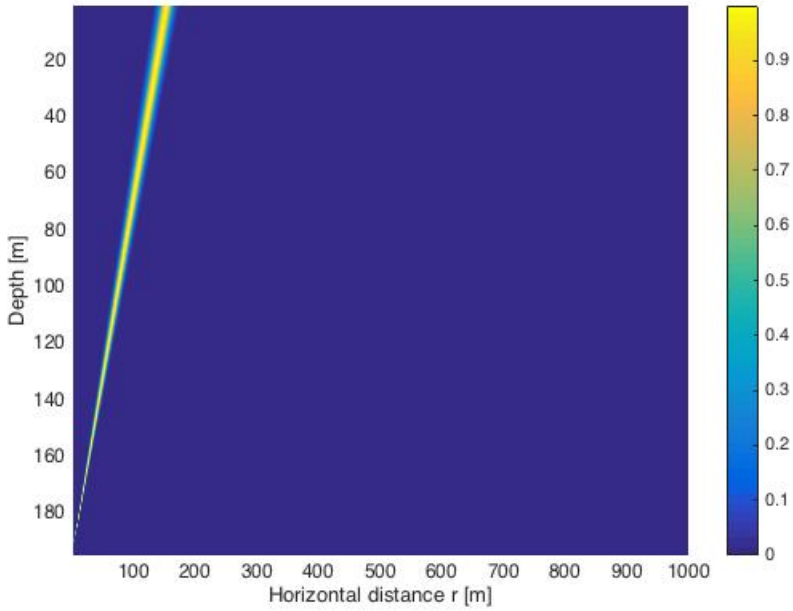

Figure 5.7: Ambiguity based on extracted $TDOMA$ at CPA

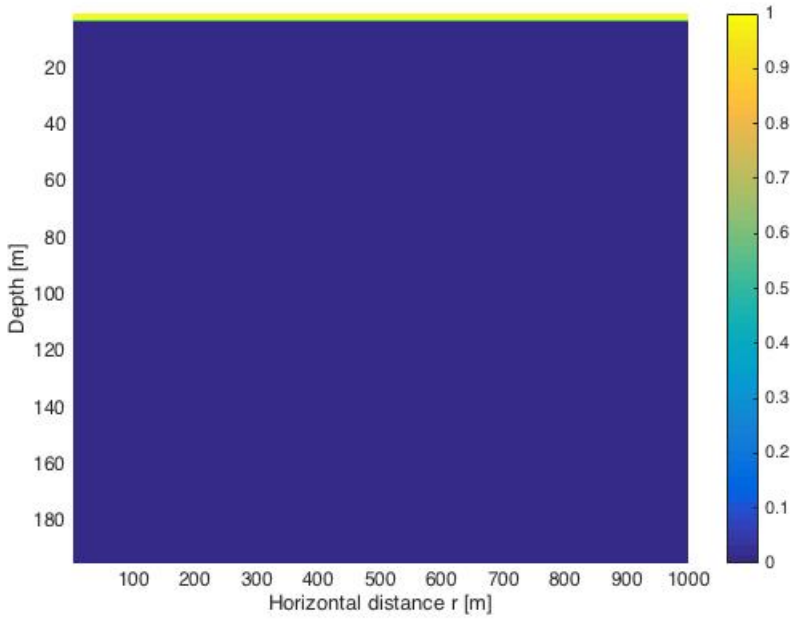

Figure 5.8: Surface vessel source depth uncertainty

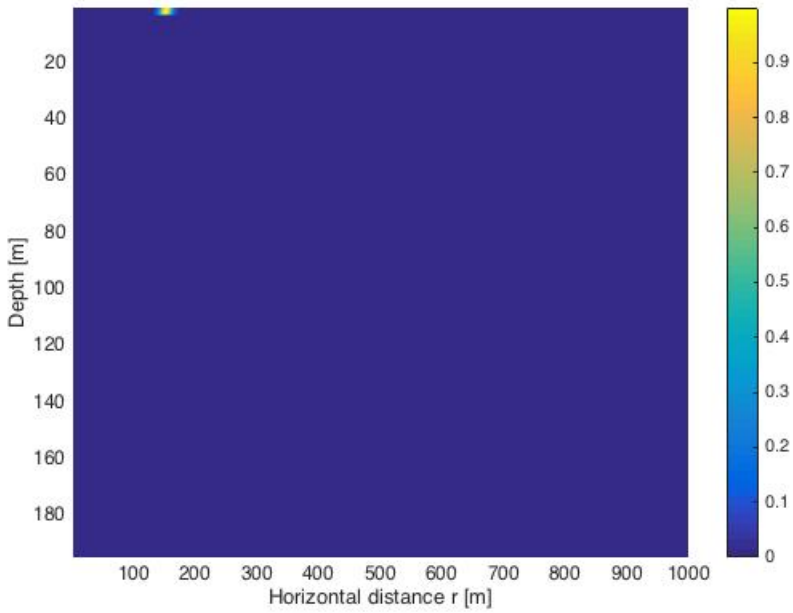

Figure 5.9: Product of source depth uncertainty and ambiguity function

The range algorithm produced the range estimate shown i Figure 5.10. These range estimates are also listed in table A.2. It shows a typical range curve for a ship passing CPA. The CPA value deviates from the CPA measured on AIS with 6m. This may be caused by errors in the geometry. The hydrophones being slightly above the seafloor, or it can be the effect of refraction by variations in the true sound speed profile not included in the model.

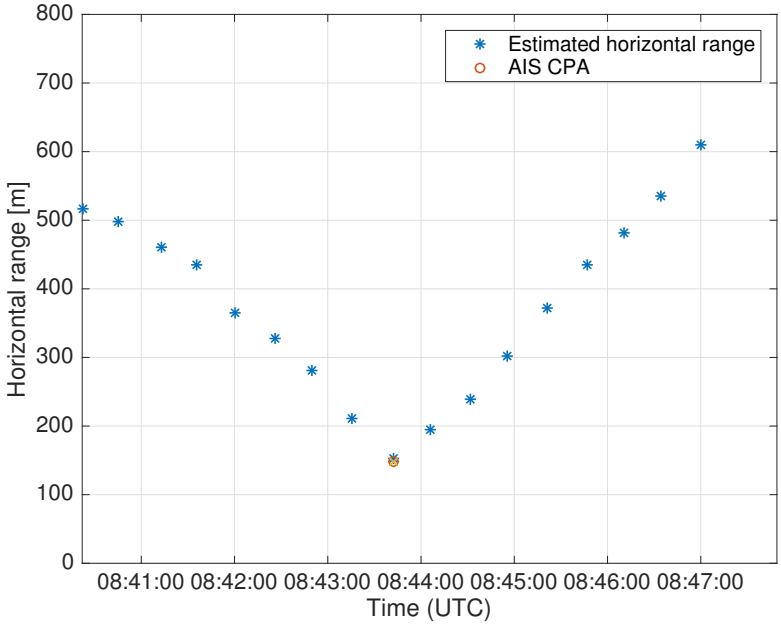

Figure 5.10: Estimated horizontal range to Wilson Goole

5.1.2 Wilson Husum

Figure 5.11: Wilson Husum

Figure 5.11 shows the cargo ship Wilson Husum. Even though Wilson Husum is physically similar to Wilson Goole, the spectrum in Figure 5.12 shows that the acoustic noise bandwidth is less and the noise is concentrated around low frequencies. The bandwidth in the ambiguity function was set to 2000Hz.

Table 5.3: AIS data Wilson Husum

CPA	105 m
Class	Merchant vessel
Draft	5.8 m
Speed	12,3 m/s

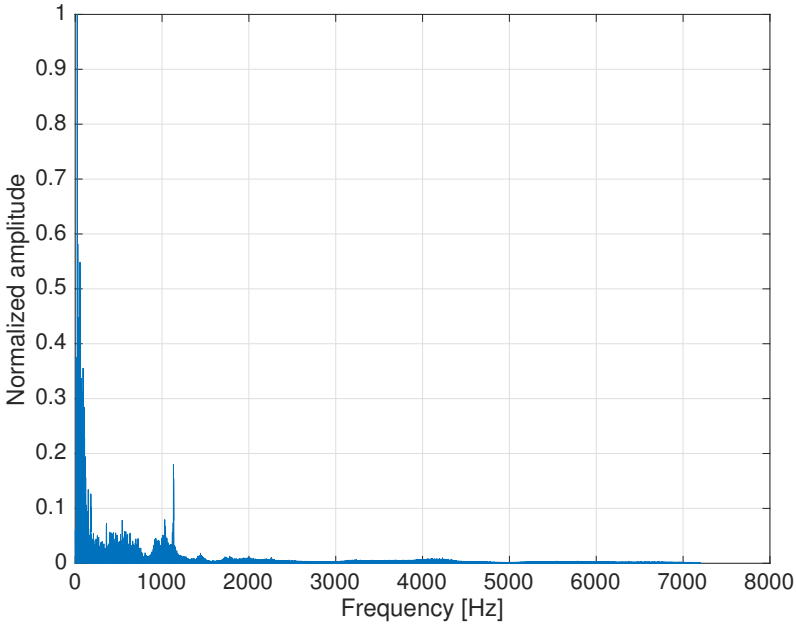

Figure 5.12: Frequency spectrum of noise from Wilson Husum

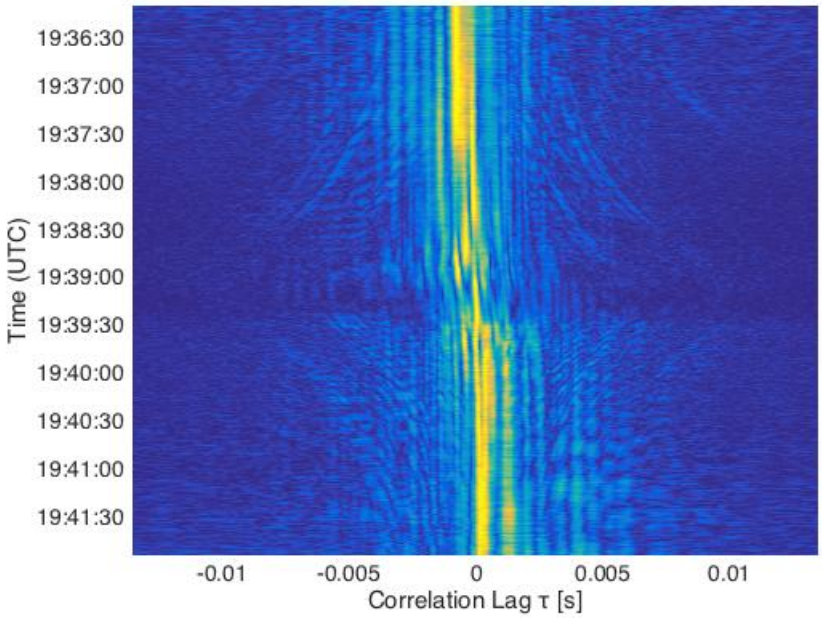

Figure 5.13: Correlogram from Wilson Husum

Figure 5.13 shows the correlogram for the merchant vessel Wilson Husum. The TDOMA lines show, and a small shift in the TDOA around $\tau = 0$ when the ship passes CPA. The effective sensor separation was set to 0.3m. The TDOMA correlation line is more difficult to follow in this correlogram than Wilson Goole. Nevertheless, with some analytic knowledge of the TDOMA function the lines were extracted into Figure 5.14. It was the inner two TDOMA lines that gave physical meaning when compared to possible TDOMA values in this channel geometry. The two outer are assumed to be the effect of ringing. These measurements were given to the range algorithm which produced the range estimates shown in Figure 5.15 and table A.3 in the appendix. This is also a typical range curve for a ship passing CPA. The range at CPA is very close to the one given by the AIS-data, deviating by only 2m .

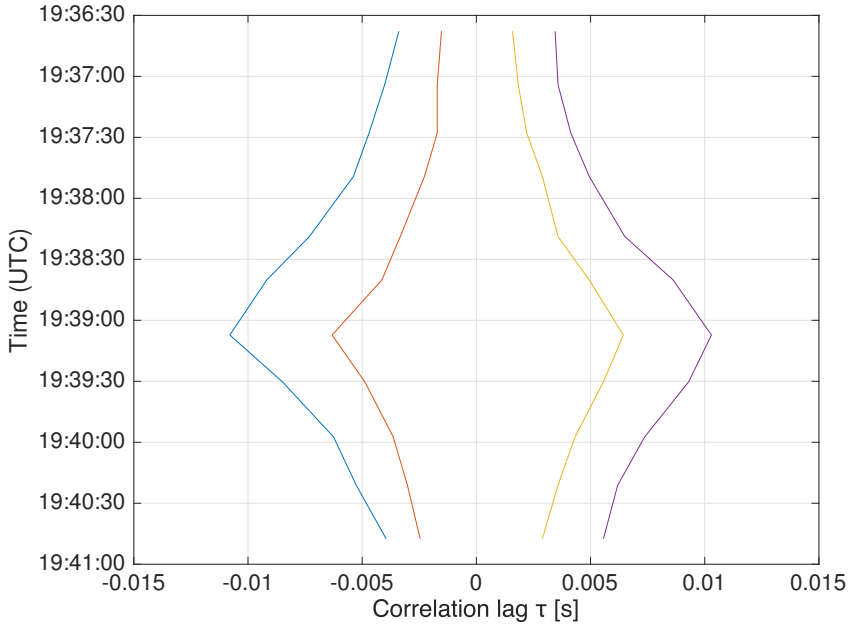

Figure 5.14: Extracted TDOMA from correlogram

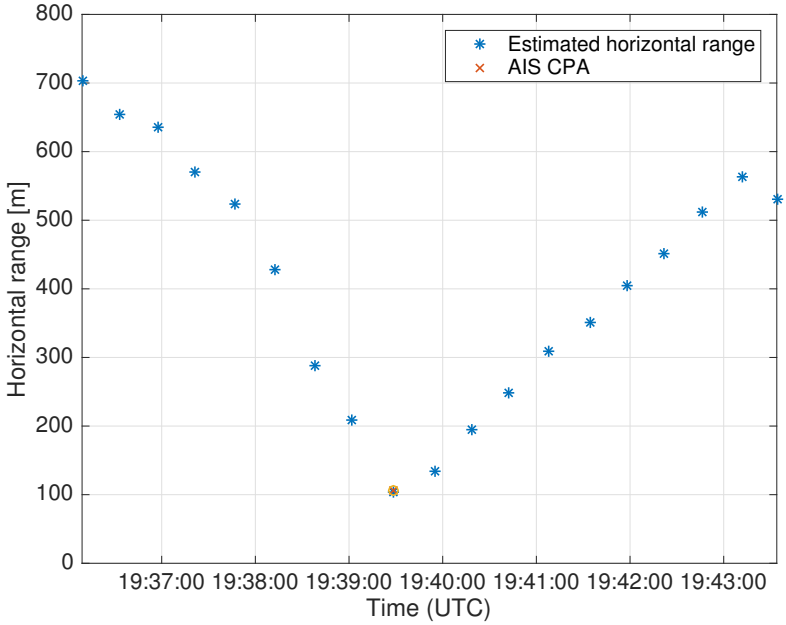

Figure 5.15: Estimated horizontal range to Wilson Husum

5.2 Vealøs 24 June 2014

The channel parameters for the Vealøs data are listed in table 5.4. The ray trace, sound speed profile and eigenrays are shown in Figures 5.16-5.17 and the ray trace shows that there is a layer at approximately 5m causing a lot of sound energy to be trapped between the reflecting surface and the layer. The source is placed at a depth of 2m and the receiver is in the eigenray example placed at 300m. The eigeray plot shows that the direct ray does not reach the receiver. This is not ideal for this ranging method since only the most vertical directed rays breaks through the layer, causing shadow zones from the surface reflected rays outside of approximately 100m. This is probably also the reason that only one recording provided correlogram that show any TDOMA. It shows the bottom and surface reflected rays, being less dependent on the exact source depth as discussed in Chapter 4. The other recordings from this data set only show the TDOA correlation with minimal variations around $\tau = 0$, and are not presented since this dynamic gives no bearing or ambiguity information. The source depth for the small boats was uniformly set to 2m given no other available information.

Table 5.4: Channel parameters Vealøs

Depth	16 m
Receiver depth	16 m
Source depth	2 m

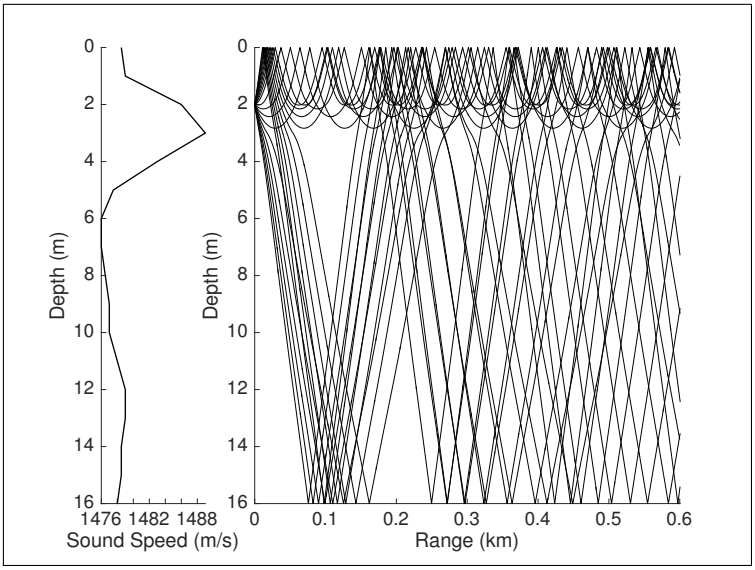

Figure 5.16: Bellhop ray trace from Vealøs

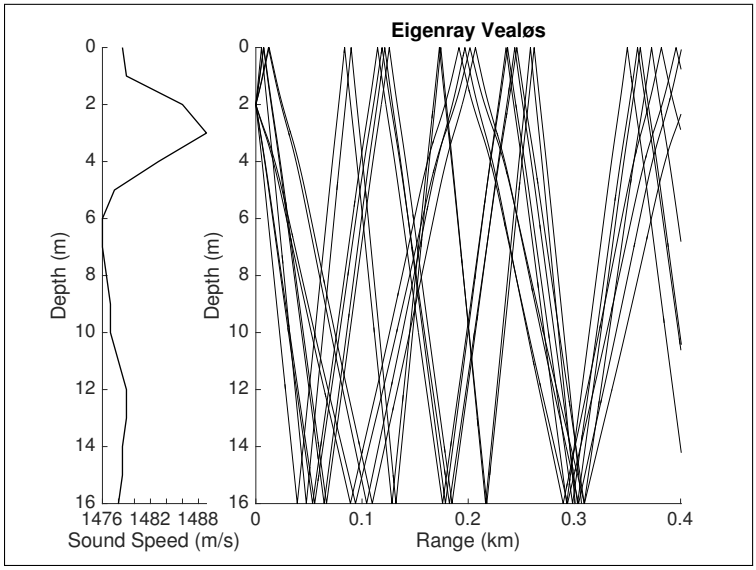

Figure 5.17: Bellhop eigenray computation from Vealøs

5.2.1 Day cruiser

Figure 5.18: Day cruiser

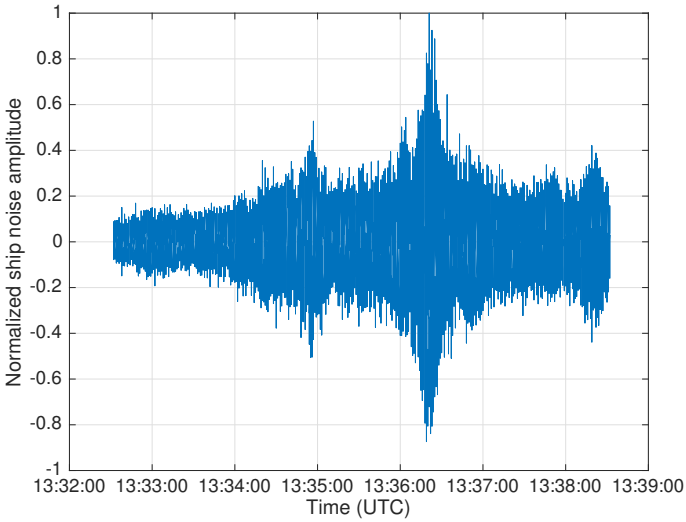

Figure 5.19: Noise signal of unknown vessel and Day Cruiser

A picture of the day cruiser is shown in Figure 5.18. The hydrophone recordings for the day cruiser are shown in Figure 5.19. These recordings were interfered with by an unknown second boat passing the Nilus sensor node prior to the day cruiser. There are no meta data on this vessel, however its noise produced TDOMA readings. This is shown in Figure 5.22. It was ranged to be further away than the day cruiser. This is not unlikely seeing the normalized signal amplitudes of each passing. Of course the smaller amplitudes of the first passing can also be caused by the simple fact that this vessel is more quiet. The normalized spectrum of both the unknown vessel and the day cruiser are shown in Figures 5.20-5.21. They probably have some of the noise of each other included in the spectrum. Note that these are normalized signal spectrum, and that one strong frequency component may give the impression that a spectrum is stronger than another. The unknown vessel has a noise bandwidth of 5000Hz and the day cruiser approximately 4000Hz which was also used in the ambiguity function.

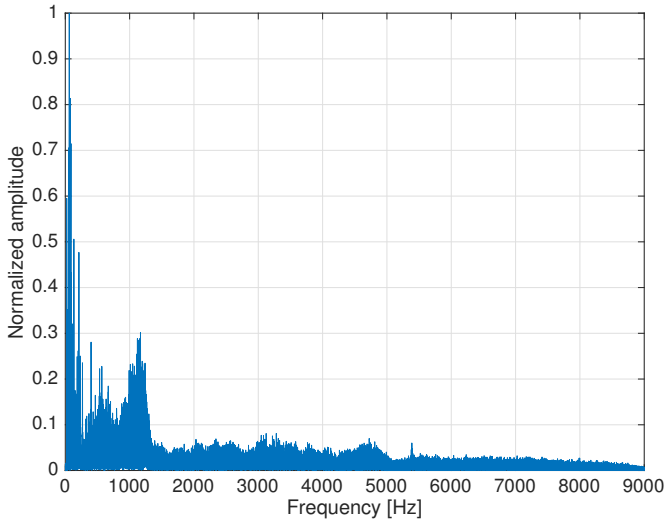

Figure 5.20: Frequency spectrum of noise from unknown vessel

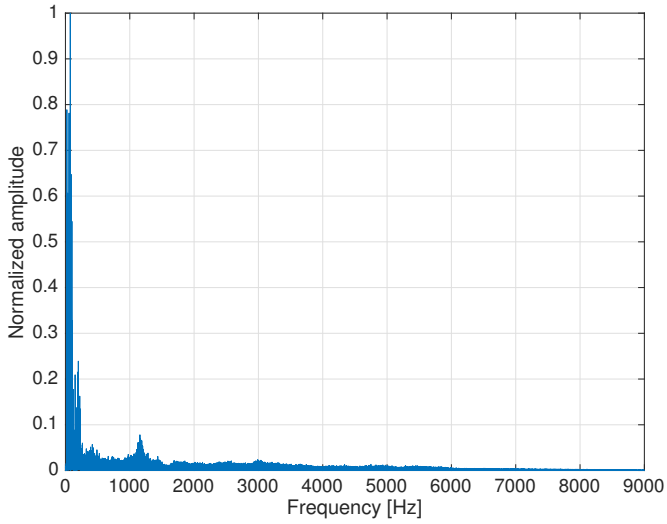

Figure 5.21: Frequency spectrum of noise from Day Cruiser

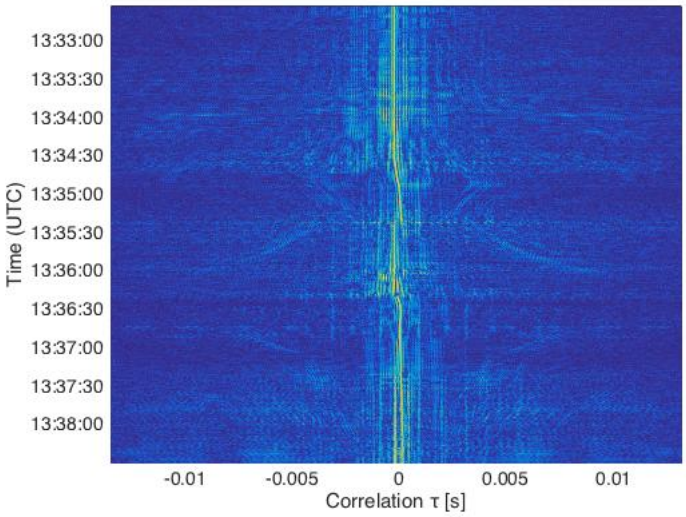

Figure 5.22: Correlogram of Day Cruiser and unknown vessel

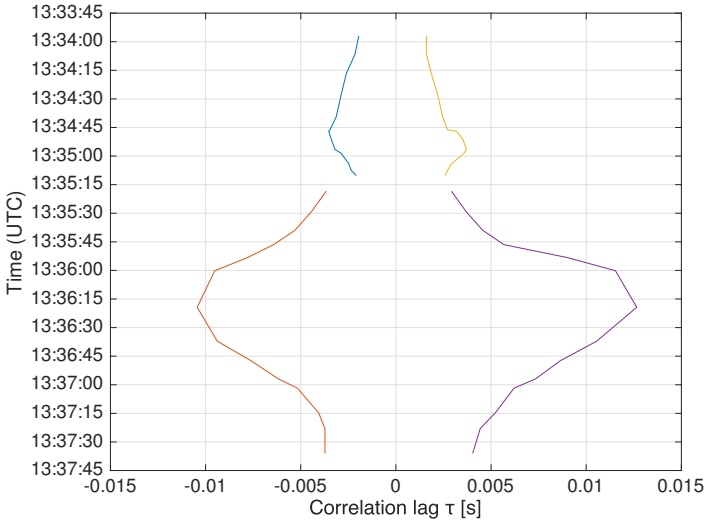

Figure 5.23: Extracted TDOMA from correlogram

The TDOMA was extracted into Figure 5.23. These extracted values gave range estimates of both the unknown vessel and the day cruiser shown in Figures 5.24-5.25. These range estimates are also listed in tables A.4-A.5 in the appendix. Both show curves of a boat passing CPA. The estimated CPA distance of the day cruiser was the same as the laser measurement.

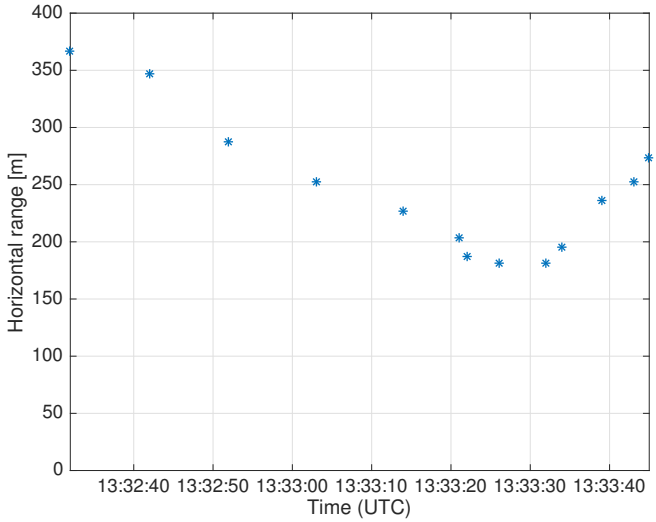

Figure 5.24: Estimated horizontal range to unknown vessel

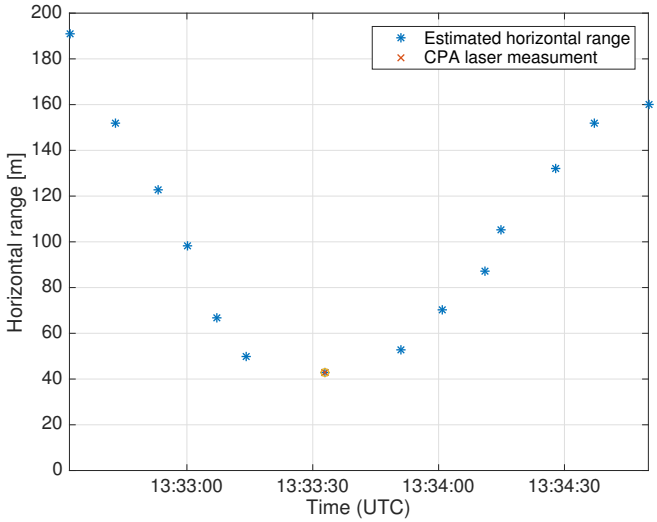

Figure 5.25: Estimated horizontal range to Day Cruiser

5.3 Estimation uncertainties

The effective hydrophone separation distance was not possible to estimate, hence this imposes error in the ray model. Another uncertainty is the source depth that was assumed 2m on the Vealos data, and the draught of the ship minus 0.5m on the NGAS data. Also the AIS distance is calculated from AIS transmitter to receiver and on large merchant vessels the AIS transmitter may be located far from the propeller. The laser measurement tool used in the Vealøs data is very accurate, but missing the boat of interest and hitting something in the vicinity may give erroneous results. Also the position of the laser measurement introduces inaccuracies because mooring exactly on top of the sensor node is difficult.
As described in chapter 4, the hydrophone spacing combined with the sample rate at this data provides insufficient TDOA data to be able to read bearing and effective hydrophone separation distance. Therefore the effective separation distance was set to 0.3m.

Chapter 6

Summary and discussion

A method for ranging of an acoustic source based on time difference of broadband noise multipath arrivals measured on two hydrophones has been developed and applied to data from two data sets. The data tested has not been ideal in both the physical limitations of the sensor node, environmental parameters as well as time resolution limitations. Studying two different data sets has revealed some common and some case dependent limitations, and more important possibilities using this method.

- First, bearing estimation providing the effective sensor separation would make it possible to correct the effective sensor separation. With the given sensor geometry and sample rate, the time resolution is not sufficient to provide bearing estimates from TDOA measurements. This makes it both impossible to localize a target in all dimensions, as well as making the correct TDOMA-tables for range estimation. This could be solved by increasing the sensor separation on the sensor node and or increase the sample rate. One simple way to increase the sensor geometry would be to deploy two Nilus sensor nodes with wired or wireless connection keeping a common clock.
- Second, all combinations giving TDOMA values converge as the horizontal range increases. Thus, this method is best for near-passages. This is illustrated in Figure 4.5 in Chapter 4. There is a small time dynamic in the TDOA and TDOMA tables which require as good time resolution as possible. This also depends on the channel geometry. Therefore, increasing the sample rate would give better results. Another positive effect of this, is that a higher sampling rate would make it possible to decrease the size of the snapshots without losing any frequency resolution, making them more stationary.
- Third, depending on channel parameters, signal to noise ratio and environmental parameters, additional TDOMA pairs may be readable. In most

cases, the TDOMA based on either the surface reflected or the bottom and surface reflected will be readable at the receiver. TDOMA based on the surface reflected are dependent on the source depth, and the time dynamic is narrow causing small model or measurement errors to change the range estimate. However, this parameter is more robust than the bottom and surface reflected because an ideal surface only shifts the signal phase without having any reflection loss. Also the parameter is only dependent on the source and receiver depth. The bottom does not need to be flat, as long as there are no shallows intersecting with the surface reflected rays. The bottom and surface reflected TDOMA is less dependent of source depth, and has a larger dynamic time range than the surface reflected. However, this parameter is less usable if the bottom is not flat within the area between the source and receiver. This parameter is also less robust because the bottom reflection has more reflection loss than the surface reflection. Traveling from surface to bottom twice makes the travel distance long and the absorption in the media increases which attenuates these rays. Therefore a better signal to noise ratio is desired.

- Fourth, placing the sensor node above the seabed would allow for TDOMA from bottom reflected rays. An ambiguity function based on the surface reflected ray and bottom reflected ray will produce unambiguous range estimates even without the source depth being known. This was studied in my project work, and further details can be viewed there [13].
- Finally, the sound speed profiles in both data sets are far from ideal. They both have a typical "summer profile" characterized by the increased sound speed near the surface due to sun heated water. The profile from Breiangen also shows the effect of rising pressure and salinity in deeper water. The ray trace from Vealøsflaket shows that a lot of the sound is trapped between the layer and the surface. Ideally this method should be tested on data from a more isotropic environment. Recordings may be performed in the same area, but the winter season would facilitate a more isovelocity sound profile.

Chapter 7

Conclusion

A model based source range estimation method for use on the Nilus sensor node has been developed. Based on measurements and modeling of time of arrival, the close range interference pattern of a noise source (ship), a localization algorithm providing plausible results was developed. The results obtained with two data sets demonstrate that a two hydrophone set up can provide good source range estimates. With small changes these sensor nodes could be able to give improved range estimates. Based on the results achieved and discussed in this work I suggest that:

1. The sensor and or hydrophone separation should be increased to get TDOA readings
2. The sample rate should be higher to get better time resolution and to reduce snapshot lengths
3. Future data should be collected in a more isotropic environment with as hard bottom as possible
4. The sensor node should be placed at a known depth above the seabed. Providing theoretically twice as many multipath arrivals carrying range information

Further studies should work on implementing effective automated trackers for measuring TDOA and TDOMA in real time. These trackers should also be smart enough to identify the different arriving TDOMA based on phase shift and statistical knowledge of these parameters. There is also a need for an algorithm to effectively swap between channels on the sensor node, always providing optimal sensor orientation. Together this would make it possible to track a target in 3 dimensions.

Bibliography

[1] Brekhovskikh and Lysanov. *Fundametals of Ocean Acoustics*, pages 101 – 103. AIP press, 3rd edition, 2003.

[2] G. Clifford Carter and Albert H. Nuttall. On the weighted overlapped segment averaging method for power spectral estimation. In *Proceedings of the IEEE*, volume 68, pages 1352 – 1354. Acoustical Society of America, 1980.

[3] Michael D. Collins. *Users's Guide for RAM Versions 1.0 and 1.0p.* Naval Research Laboratory, Washington, DC, 20375, May 1999.

[4] Brian G. Ferguson and Kam W. Lo. Monitoring the underwater acoustic pressure field using two spatially-separated hydrophones with application to forward-aft sensors onboard an undersea glider. *2nd International Confrence and Exibition on Underwater Acoustics*, 2014.

[5] John Gebbie. Personal communication.

[6] M. McCargar R. Allen JS. Gebbie, J. Siderius and G Pusey. Localization of a noisy broadband surface target using time differences of multipath arrivals. *JASA Express Letters*, 2013.

[7] J. M. Hovem. *Marine Acoustics - The Physics of Sound in Underwater Environments*, pages 130 – 137. Peninsula Publishing, 1 edition, 2012.

[8] Charles H. Knapp and G. Clifford Carter. The generalized correlation method for estimation of time delay. In *Transactions on acoustics, speech, and signal processing*, volume ASSP-24, page 33 – 36. IEEE, 1976.

[9] Frank R. Kschishang. The hilbert transform. Technical report, University of Toronto, The Edward S. Rogers Sr. Department of Electrical and Computer Engineering, 2006.

[10] Roald Otnes. Nilus – an underwater acoustic sensor network demonstrator system. Paper presented at 10th International Mine Warfare Technology Symposium, Monterey, CA, USA, 2012.

[11] Michael B. Porter. *The BELLHOP Manual and User's Guide.* Heat, Light, and Sound Research Inc. La Jolla CA, USA, 2011.

[12] John G. Proakis and Dimitris G. Manolakis. *Digital Signal Processing - Principles, Algorithms, and Applications*, pages 625–636. Pretice-Hall Inc., third edition, 1996.

[13] Narve Garshol Skurtveit. Source range estimation using hydrophone data from an ocean glider. Technical report, Norwegian University of Science and Technology, December 2015.

[14] Discovery Of the Sound In The Sea. Ship noise. `http://www.dosits.org/resources/all/featuresounds/shipnoise/`. The University of Rhode Island, Accessed 2016-06-02.

[15] A.D. Waite. *Sonar for Practising Engineers*, pages 125–159. John Wiley & Sons Ltd, 3 edition, 2002.

[16] Dr Salih Salih Yi-Wen Liu. *Hilbert Transform and Applications, Fourier Transform Applications*. InTech, 1 edition, 2012.

Appendix A

Additional results

The range estimates presented in Chapter 5 are listen in tables A.2-A.5.
The method produced was tested on additional data at FFI. Results from this work may be made available upon request to FFI. The Matlab code for producing the correlogram and range estimates may be provided upon request by sending an e-mail to: narve.garsholskurtveit@gmail.com

AIS meta data and time relevant time variables to navigate the trial recordings are listed in table A.1.

Table A.1: AIS data and time estimations to identify correct vessel in recordings

Trial	Receiver	Depth	DTG	CPA-time	Vessel	CPA	Vessel type	Speed	Draught
NGAS10	NILUS1 (A)	195m	100610-070556	07:54:52	Wilson Goole	147	MV	11,6	5.8 m
NGAS10	NILUS1 (A)	195m	100610-154608	19:45:48	Wilson Husum	105	MV	12,3	5.8 m
VEAL14	NILUS2	15.6m	140624-072832	13:33:26	Day cruiser	43	Pleasure craft	-	-

A.1 NGAS - 10.June 2010

Table A.2: Etimated horizontal range to Wilson Goole

Time (UTC)	08:40:22	08:40:45	08:41:13	08:41:36	08:42:00	08:42:26	08:42:50	08:43:16	08:43:42	08:44:06
Range [m]	517	499	461	436	365	328	281	211	153	194
Time (UTC)	08:44:32	08:44:55	08:45:21	08:45:47	08:46:11	08:46:34	08:47:00	08:47:26	08:47:49	
Range [m]	239	303	373	436	482	536	610	725	825	

Table A.3: Estimated horizontal range to Wilson Husum

Time (UTC)	19:36:09	19:36:33	19:36:58	19:37:21	19:37:47	19:38:13	19:38:38	19:39:02	19:39:28	19:39:55
Range [m]	703	654	635	571	524	427	289	208	103	134
Time (UTC)	19:40:19	19:40:42	19:41:08	19:41:35	19:41:58	19:42:22	19:42:46	19:43:12	19:43:34	
Range [m]	194	248	309	351	405	451	511	564	530	

A.2 Vealøs - 24.June 2014

Table A.4: Estimated horizontal range to Unknown vessel

Time (UTC)	13:32:32	13:32:42	13:32:52	13:33:03	13:33:14	13:33:21	13:33:22	13:33:26
Range [m]	367	347	287	252	227	204	187	181
Time (UTC)	13:33:32	13:33:34	13:33:39	13:33:43	13:33:45			
Range [m]	181	195	236	252	274			

Table A.5: Estimated horizontal range to Day Cruiser

Time (UTC)	13:32:32	13:32:43	13:32:53	13:33:00	13:33:07	13:33:14	13:33:33
Range [m]	191	152	123	98	67	50	43
Time (UTC)	13:33:51	13:34:01	13:34:11	13:34:15	13:34:28	13:34:37	13:34:50
Range [m]	53	70	87	105	132	152	160

Appendix B

Validation of the ray model

The ray model purposed by Brekhovskikh [1] was coded and verified in my project thesis [13]. Different channel parameters was studied in this work. The results from the ray model was compared with data simulated by RAM and Bellhop [3][11]. These two recognized programs compute sound field data and arrivals times. To briefly summarize this work, both the transmission loss and the time arrivals match these models in an isotropic environment . This is shown in Figure B.1 and Figure B.2. Model parameters to produce these results are listed in table B.1. The arrivals in Figure B.2 show the direct first arrival to the most left, the 1st- 2nd-, 3rd-reflected and so on are shown chronological from left to right.

Table B.1: Model parameters

f	100 Hz	r	1-1000 m
d_w	100 m	d_s	5 m
ρ_1	1000 kg/ms	c_1	1500 m/s
ρ_2	1250 kg/ms	c_2	1700 m/s
d_r	20	rays	20

B.1 Isotropic environment

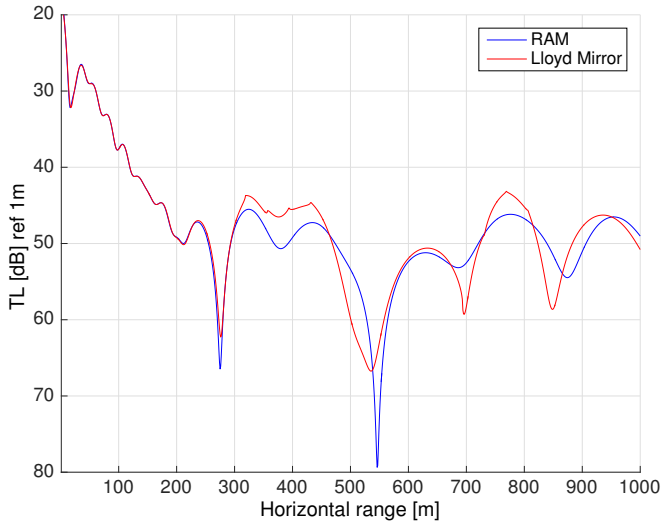

Figure B.1: Transmission loss of Lloyd Mirror and RAM compared

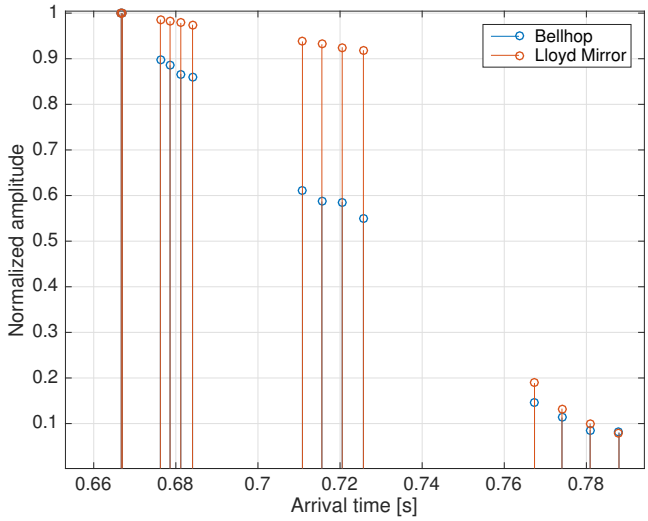

Figure B.2: Time arrival Bellhop and Lloyd Mirror compared

Comparison of transmission loss and arrival time with varying sound speed profiles and bathymetry was also computed. The transmission loss of the LM model matches in most cases to a range of 250 m, which is a rather short range. Thus, inversion based on transmission loss from a source beyond this range may produce erroneous results. If the environment is isotropic the time arrivals will match, where as the pressure field has small deviations after 250. Therefore, ranging based on time difference of arrival most likely provides a better range estimate than field inversion. Nevertheless, in cases where the sound speed has large variations, range estimation based on time differences of arrival will also be challenging.